

Stochastic induced gravitational waves and lowest mass limit of primordial black holes with the effects of reheating

Nilanjandev Bhaumik and Rajeev Kumar Jain

Department of Physics, Indian Institute of Science, Bangalore 560012, India

E-mail: nilanjandev@iisc.ac.in, rkjain@iisc.ac.in

Abstract. Recently, we have studied the abundance of primordial black holes (PBH) produced in a single field inflationary model with a polynomial potential containing even powers up to the sextic order which allows the existence of an inflection point in the inflaton potential. We found that such a scenario can produce PBHs in a wide range of masses with a nearly monochromatic mass fraction which can account for the total dark matter of the universe in the asteroid mass window. In this paper, we study the stochastic background of gravitational waves (GW) which is inevitably generated in this scenario due to the second order effects caused by large primordial scalar curvature perturbations at the PBHs scales. We find that the resulting secondary background of GWs could be potentially detected by the future space based GWs observatories such as LISA, TAIJI, DECIGO or BBO. Using a model independent approach, we also obtain a lower limit on the PBHs mass by only assuming an instantaneous and a smooth transition from the ultra slow roll to the slow roll phase. Further, we investigate the effects of reheating on the secondary GWs spectrum and find that an epoch of a non-instantaneous reheating can cause a shift in the GWs spectrum to larger frequencies. Interestingly, in this scenario, we also notice that very light PBHs which may completely evaporate by today and would not contribute to the dark matter at all, will still generate a stochastic background of secondary GWs that may be detected by a future design of the ground based Advanced LIGO detector.

Keywords: Inflation, Primordial black holes, Gravitational waves, Dark matter

Contents

1	Introduction	1
2	Stochastic GWs from second order scalar perturbations	3
2.1	Basics of GWs power spectrum and energy density	3
2.2	Induced tensor modes and their power spectrum	4
2.3	The present spectral energy density of GWs	6
2.4	The spectral tilt of the induced GWs spectrum	9
3	Observing ultralight PBHs with Advanced LIGO	12
4	A lower bound on the PBHs mass for USR inflation	14
4.1	An instantaneous transition from USR to SR	14
4.2	A smooth transition from USR to SR	15
4.3	Estimation of the lower bound on the PBHs mass	18
5	Imprints of reheating on the secondary GWs spectrum and the lower mass bound	20
6	Conclusions and discussions	22

1 Introduction

Primordial black holes (PBH) are now widely considered one of the most interesting candidate to explain the entire cold dark matter (CDM) in the universe and have gained a lot of attention lately, thanks to the recent detection of astrophysical gravitational waves (GW) from a system of binary black holes, as reported by the LIGO-Virgo scientific collaboration [1–6]. Moreover, it has been discussed that super massive black holes which are observed at the centre of massive galaxies at high redshifts could have been originated from the distribution of PBHs [7–10]. It is well known that PBHs can be produced in the early universe, particularly, after inflation when primordial curvature perturbations with large overdensities re-enter the horizon during the radiation dominated (RD) epoch [11–14]. Lately, a large number of inflationary models have been studied to produce PBHs in different mass ranges, in particular, the class of models producing PBHs in the asteroid mass window in which PBHs could contribute to the total CDM in the universe [15–37].

A stochastic background of primordial gravitational waves (GW) is a central prediction of all the inflationary models and in particular, a nearly scale invariant spectrum of tensor perturbations is widely regarded as the holy grail of single field inflationary models. Such a background encodes pivotal information which can be used to probe and constrain the physics of the early universe and fundamental physics operating at very high energies. It has been well known that in single field slow roll inflationary models, the stochastic GWs background is nearly scale invariant which is usually generated from the amplification of vacuum tensor fluctuations at the linear order wherein the inflaton field is the only dynamical degree of freedom. However, models with many dynamical fields such as extra spectator fields or gauge fields also lead to a secondary background of GWs with very different properties

and characteristics than the vacuum contribution. Distinct signatures of such a background can then be used to probe a general class of inflationary scenarios beyond the single field inflationary models. Besides probing the fundamental physics of the early universe, the spectral energy density of inflationary GWs at the present epoch can also be used to trace and probe the thermal history of the universe [38–43]. For some recent reviews on various cosmological backgrounds of GWs, their generation and their detection, see refs. [44, 45].

In general, a cosmological background of GWs at the second order through mode coupling of scalar metric perturbations is always generated in all the inflationary models. Since the power spectrum of second order metric perturbations should be of order 10^{-18} in the RD era, one can expect that this GWs background to be extremely small and is quite far from the reach of present and upcoming GWs observatories. However, in all the inflationary scenarios of PBHs formation, since the power spectrum of scalar curvature perturbations must be enhanced at smaller scales to produce PBHs, this secondary GWs background typically turns out to be quite large and is therefore, considered an interesting and relevant byproduct of all such inflationary scenarios [46–62].

In an earlier paper [32], we had studied an inflationary scenario with a sextic order polynomial potential that allows the existence of an inflection point in the inflaton potential. Such a potential allows an epoch of an ultra slow roll (USR) evolution which leads to an enhancement of the spectrum of primordial scalar curvature perturbations at small scales. We found that this scenario can produce PBHs in different mass ranges and in particular, in the asteroid mass range in which PBHs can contribute to the entire CDM. In this paper, we shall study the induced background of stochastic GWs in this scenario which is generated from the contribution due to mode coupling of second order scalar perturbations to the inflationary tensor perturbations. Such GWs are generated on smaller scales after they re-enter the horizon during the RD phase. We shall calculate this induced GWs background in our model which is produced in a range of different frequencies, using an adequate numerical approach and compare it with the current and projected sensitivities of various ground and future space based GWs observatories. Interestingly, we find that in most cases of our model, the produced GWs background can be simultaneously detected by different GWs observatories which is usually not the case when the primordial power spectrum is highly peaked. We emphasise that this feature provides a unique opportunity to constrain the signal much better. In models which produce PBHs in the asteroid mass window as in our scenario, the secondary GWs background is usually peaked in the frequency band $f_{\text{GW}} \sim 10^{-3} - 1$ Hz and thus, can be potentially detected with the future space based GWs observatories such as LISA [63–66], TAIJI [67], DECIGO [68, 69] or BBO [70]. Moreover, we also notice an interesting observational possibility that very light PBHs produced in our scenario with mass $M_{\text{PBH}} \sim 10^{-20} - 10^{-21} M_{\odot}$ which would have been completely evaporated by today, would still lead to an induced GWs background at larger frequencies which can, in principle, be observed by the future design of the ground based Advanced LIGO detector [71].

Using a model independent approach, we shall also obtain a lower bound on the PBHs mass in our case by assuming an instantaneous and a smooth transition from the USR to the slow roll (SR) phase. Our mass bounds are applicable as far as there is no intermediate fast roll stage between the USR and the SR phase. Furthermore, we shall also study the effects of reheating after the end of inflation on this GWs background and find that a prolonged epoch of a non instantaneous reheating leads to a shift in the GWs energy spectrum while the shape of the spectrum remains invariant. Thus, such induced GWs signal can be detected simultaneously by different GWs observatories.

The remainder of this paper is organised as follows: In the following section, we shall quickly discuss the basic formalism to compute the secondary background of GWs from second order scalar perturbations in any general inflationary scenario. We shall compute the spectral energy density of GWs today for the scenario of PBHs formation that we had presented in our earlier work and compare it with the optimal (design) sensitivities of various present and future GWs observatories. In Section 3, we shall discuss that secondary GWs induced by ultralight PBHs can be detected by a future run of ground based Advanced LIGO detector. In Section 4, we shall discuss how to obtain the lowest possible PBHs mass both for the cases of an instantaneous transition and a smooth transition from the USR to the SR phase. In Section 5, we shall study the resulting effects of a non instantaneous reheating epoch on the GWs spectra and the lower bound on the PBHs mass. Finally, we shall summarise our results and discuss their implications in Section 6.

Our conventions and notations adopted in this paper are as follows. We work in the natural units, $\hbar = c = 1$, with reduced Planck mass $M_{\text{Pl}}^2 = (8\pi G)^{-1}$. Our metric signature is mostly plus with $(-, +, +, +)$. The background metric is described by the homogeneous, isotropic and spatially flat FLRW universe with a line element $ds^2 = -dt^2 + a^2(t)d\mathbf{x}^2 = a^2(\tau)(-d\tau^2 + d\mathbf{x}^2)$. The conformal time τ is defined as $d\tau = dt/a(t)$. The overdots and primes denote the derivatives with respect to the cosmic time t and the conformal time τ , respectively. The Hubble parameter is defined as $H \equiv \dot{a}/a$ while the conformal Hubble parameter is given by $\mathcal{H} \equiv aH \equiv a'/a$.

2 Stochastic GWs from second order scalar perturbations

It is well known that, at the linear order in perturbations, the scalar, vector and tensor perturbations evolve independently, thanks to the decomposition theorem and their evolution is governed by their corresponding equations of motion. In particular, the vector perturbations simply decay in an inflating universe. However, at the second order in perturbations, an extra source term is generated for the tensor perturbations due to the mode coupling of scalar metric fluctuations which inevitably leads to a secondary background of induced GWs. In this section, we shall present the basic formalism and essential equations for the tensor perturbations with a source term due to second order scalar perturbations. We shall then solve these equations numerically for the inflationary scenario that we had discussed in our earlier work [32] and present the GWs energy density spectrum calculated at the present epoch. We shall also discuss the potential detection of this secondary GWs background with the future space based GWs observatories such as LISA, TAIJI, DECIGO or BBO.

2.1 Basics of GWs power spectrum and energy density

In this section, we shall closely follow the discussion of the seminal paper [46]. Let us start with perturbing the FLRW metric with the scalar and tensor perturbations. In the conformal Newtonian gauge, the perturbed metric can be written as

$$ds^2 = -a^2(\tau)(1 + 2\Phi) d\tau^2 + a^2(\tau) \left[(1 - 2\Psi)\delta_{ij} + \frac{1}{2}h_{ij} \right] dx^i dx^j, \quad (2.1)$$

where Φ and Ψ are the scalar metric perturbations, also called the Bardeen potentials and h_{ij} is the tensor perturbation which is symmetric ($h_{ij} = h_{ji}$), traceless ($h_{ii} = 0$), and transverse ($h_{ij,j} = 0$). Under the assumption $\Phi = \Psi$, the scalar part of the anisotropic stress (shear) vanishes but the corresponding tensor part does not. As we shall see later, this serves as a

source to the evolution equation for tensor perturbations. Furthermore, one can rewrite h_{ij} in terms of the basis $\{e_{ij}^+(\mathbf{k}), e_{ij}^\times(\mathbf{k})\}$ of polarisation tensors as follows

$$h_{ij}(\tau, \mathbf{x}) = \int \frac{d^3k}{(2\pi)^{3/2}} \left[e_{ij}^+(\mathbf{k}) h_{\mathbf{k}}^+(\tau) + e_{ij}^\times(\mathbf{k}) h_{\mathbf{k}}^\times(\tau) \right] e^{i\mathbf{k}\cdot\mathbf{x}}, \quad (2.2)$$

where $e_{ij}^+(\mathbf{k}) = \frac{1}{\sqrt{2}}(e_i(\mathbf{k})e_j(\mathbf{k}) - \bar{e}_i(\mathbf{k})\bar{e}_j(\mathbf{k}))$ and $e_{ij}^\times(\mathbf{k}) = \frac{1}{\sqrt{2}}(e_i(\mathbf{k})\bar{e}_j(\mathbf{k}) + \bar{e}_i(\mathbf{k})e_j(\mathbf{k}))$, with $e_i(\mathbf{k})$ and $\bar{e}_i(\mathbf{k})$ being normalised three-dimensional vectors orthonormal to \mathbf{k} . With the Fourier modes $h_{\mathbf{k}}$, one can now define the dimensionless power spectrum \mathcal{P}_h as

$$\frac{k^3}{2\pi^2} \langle h_{\mathbf{k}}^\lambda(\tau) h_{\mathbf{k}'}^{\lambda'}(\tau) \rangle = \delta_{\lambda\lambda'} \delta^3(\mathbf{k} + \mathbf{k}') \mathcal{P}_h(\tau, k), \quad (2.3)$$

where $\lambda, \lambda' = \{+, \times\}$ represent the two polarisations of tensor perturbations. Now, the GWs energy density per logarithmic wavelength can be defined as

$$\Omega_{\text{GW}}(\tau, k) \equiv \frac{1}{\rho_c} \frac{d\rho_{\text{GW}}}{d \ln k} = \frac{\rho_{\text{GW}}(\tau, k)}{\rho_{\text{tot}}(\tau)} = \frac{1}{24} \left(\frac{k}{\mathcal{H}} \right)^2 \overline{\mathcal{P}_h(\tau, k)}, \quad (2.4)$$

where the overline denotes an average over time. This energy density Ω_{GW} at the present epoch $\tau = \tau_0$ is an observationally relevant quantity which can be calculated using the power spectrum \mathcal{P}_h . Note that, in parity invariant scenarios as in our model, both the polarisations will lead to the same result for the GWs spectrum. However, in parity violating situations, the power spectrum will be different for the two polarisations. In particular, when one helicity mode is exponentially amplified due to dynamical instabilities than the other, the power spectrum turns out to be maximally helical and has very interesting observational implications. For simplicity, from now on, we shall ignore the superscript λ in $h_{\mathbf{k}}$.

2.2 Induced tensor modes and their power spectrum

Using the standard canonical quantisation procedure for h_{ij} , one finds that the equation of motion for the Fourier modes $h_{\mathbf{k}}$, sourced by the scalar perturbations Φ is given by

$$h_{\mathbf{k}}''(\tau) + 2\mathcal{H}h_{\mathbf{k}}'(\tau) + k^2 h_{\mathbf{k}}(\tau) = 4S_{\mathbf{k}}(\tau), \quad (2.5)$$

where $S_{\mathbf{k}}$ is the Fourier component of the source term comprising of second order scalar perturbations. This differential equation can be solved by the Green's function method which yields the solution as [52]

$$h_{\mathbf{k}}(\tau) = \frac{4}{a(\tau)} \int^\tau d\bar{\tau} a(\bar{\tau}) G_{\mathbf{k}}(\tau, \bar{\tau}) S_{\mathbf{k}}(\bar{\tau}), \quad (2.6)$$

where $G_{\mathbf{k}}(\tau, \bar{\tau})$ is the solution to the following equation

$$G_{\mathbf{k}}''(\tau, \bar{\tau}) + \left[k^2 - \frac{a''(\tau)}{a(\tau)} \right] G_{\mathbf{k}}(\tau, \bar{\tau}) = \delta(\tau - \bar{\tau}). \quad (2.7)$$

Since we are interested in the induced GWs background on smaller scales corresponding to $k \gg k_{\text{eq}}$ which re-enter the horizon during RD epoch, we shall restrict our following

discussion to RD epoch with $w = 1/3$ only. In that case, the source term $S_{\mathbf{k}}$ can be written as

$$S_{\mathbf{k}} = \int \frac{d^3q}{(2\pi)^{3/2}} e_{ij}^\lambda(\mathbf{k}) q_i q_j [2\Phi_{\mathbf{q}}\Phi_{\mathbf{k}-\mathbf{q}} + (\mathcal{H}^{-1}\Phi'_{\mathbf{q}} + \Phi_{\mathbf{q}})(\mathcal{H}^{-1}\Phi'_{\mathbf{k}-\mathbf{q}} + \Phi_{\mathbf{k}-\mathbf{q}})]. \quad (2.8)$$

As mentioned earlier, this source term is at the second order in $\Phi_{\mathbf{k}}$ which is the Fourier mode of Φ and is explicitly symmetric under the exchange of $\mathbf{q} \rightarrow \mathbf{k} - \mathbf{q}$. During the RD era, induced GWs are produced mainly around the horizon re-entry, without growing any further because the gravitational potential oscillates after horizon re-entry. At first order, assuming no anisotropic pressure, the time evolution of $\Phi_{\mathbf{k}}$ is governed by

$$\Phi_{\mathbf{k}}''(\tau) + 3\mathcal{H}(1 + c_s^2)\Phi_{\mathbf{k}}'(\tau) + (2\mathcal{H}' + (1 + 3c_s^2)\mathcal{H}^2 + c_s^2k^2)\Phi_{\mathbf{k}}(\tau) = 0, \quad (2.9)$$

For RD era, using $c_s^2 = w = 1/3$ and $\mathcal{H} = 1/\tau$, the above equation reduces to

$$\Phi_{\mathbf{k}}''(\tau) + \frac{4}{\tau}\Phi_{\mathbf{k}}'(\tau) + \frac{1}{3}k^2\Phi_{\mathbf{k}}(\tau) = 0, \quad (2.10)$$

which has an analytical solution as

$$\begin{aligned} \Phi_{\mathbf{k}}(\tau) &= \frac{A(\mathbf{k})}{(k\tau)^3} \left[\frac{k\tau}{\sqrt{3}} \cos\left(\frac{k\tau}{\sqrt{3}}\right) - \sin\left(\frac{k\tau}{\sqrt{3}}\right) \right] \\ &+ \frac{B(\mathbf{k})}{(k\tau)^3} \left[\frac{k\tau}{\sqrt{3}} \sin\left(\frac{k\tau}{\sqrt{3}}\right) + \cos\left(\frac{k\tau}{\sqrt{3}}\right) \right]. \end{aligned} \quad (2.11)$$

This solution will act as a source for the GWs at the second order. At early times when $k\tau \rightarrow 0$, we find that

$$\Phi_{\mathbf{k}}(\tau) = -\frac{A(\mathbf{k})}{3^{5/2}} + \frac{B(\mathbf{k})}{(k\tau)^3}. \quad (2.12)$$

Here, the first term is the constant mode *i.e.* constant in time but the second term is the decaying mode which can be neglected hereafter. We can therefore write the dominant solution for $\Phi_{\mathbf{k}}(\tau)$ in RD era as

$$\Phi_{\mathbf{k}}(\tau) = \mathcal{T}(k\tau)\tilde{\Phi}_{\mathbf{k}}, \quad (2.13)$$

where $\mathcal{T}(k\tau)$ is the transfer function in RD and its expression is given by

$$\mathcal{T}(k\tau) = \frac{9}{(k\tau)^2} \left[\frac{\sqrt{3}}{k\tau} \sin\left(\frac{k\tau}{\sqrt{3}}\right) - \cos\left(\frac{k\tau}{\sqrt{3}}\right) \right]. \quad (2.14)$$

As is well known, in the RD era, the scalar perturbation $\Phi_{\mathbf{k}}$ is directly related to the gauge invariant comoving curvature perturbation by $\tilde{\Phi}_{\mathbf{k}} = \frac{2}{3}\mathcal{R}(\mathbf{k})$ so we can now write

$$\Phi_{\mathbf{k}}(\tau) = \frac{2}{3}\mathcal{T}(k\tau)\mathcal{R}(\mathbf{k}). \quad (2.15)$$

All the details of the calculation of the induced tensor spectrum can be found in [52, 54, 72] and thus, we shall only restrict to the essential equations needed for our discussion.

One can now solve the mode equation (2.5) together with the source term given in (2.8). The final solution can be written in a compact form as

$$h_{\mathbf{k}}^s(\tau) = \frac{4}{9} \int \frac{d^3p}{(2\pi)^3} \frac{1}{k^3\tau} e^s(\mathbf{k}, \mathbf{p}) \mathcal{R}(\mathbf{p}) \mathcal{R}(\mathbf{k} - \mathbf{p}) \left[\mathcal{I}_c(v, u) \cos(k\tau) + \mathcal{I}_s(v, u) \sin(k\tau) \right], \quad (2.16)$$

where $v = p/k$, $u = |\mathbf{k} - \mathbf{p}|/k$ and

$$e^s(\mathbf{k}, \mathbf{p}) \equiv e^{s,ij}(\mathbf{k})p_i p_j = \begin{cases} \frac{1}{\sqrt{2}}p^2 \sin^2 \theta \cos 2\phi & \text{for } s = +, \\ \frac{1}{\sqrt{2}}p^2 \sin^2 \theta \sin 2\phi & \text{for } s = \times. \end{cases} \quad (2.17)$$

The analytic form of the two functions \mathcal{I}_c and \mathcal{I}_s can be found in [72]. In order to calculate the power spectrum \mathcal{P}_h from the solution (2.16), we immediately realise that it will involve the four point functions of $\mathcal{R}(\mathbf{k})$. However, noting that at leading order it is a Gaussian variable defined by the dimensionless power spectrum $\mathcal{P}_{\mathcal{R}}$ as

$$\frac{k^3}{2\pi^2} \langle \mathcal{R}(\mathbf{k})\mathcal{R}(\mathbf{k}') \rangle = (2\pi)^3 \delta^{(3)}(\mathbf{k} + \mathbf{k}') \mathcal{P}_{\mathcal{R}}(k). \quad (2.18)$$

Upon using Wick's theorem, the four point functions can be written in terms of the two point function or the power spectrum with all possible contractions. After a lot of simplification, one finds

$$\mathcal{P}_h(\tau, k) = 4 \int_0^\infty dv \int_{|1-v|}^{1+v} du \left(\frac{4v^2 - (1 + v^2 - u^2)^2}{4uv} \right)^2 I_{\text{RD}}^2(v, u, x) \mathcal{P}_{\mathcal{R}}(kv) \mathcal{P}_{\mathcal{R}}(ku), \quad (2.19)$$

where $x = k\tau$ and $x \rightarrow 0$ indicates the onset of the RD epoch. The factor I_{RD} is a very involved function and its general form can be found in [52]. For small x , the leading term of I_{RD} is independent of u and v , $I_{\text{RD}} \simeq x^2/2$. From observational point of view, one is interested in the GWs spectrum today, corresponding to the late time limit *i.e.* $x \gg 1$ which is given by

$$\Omega_{\text{GW}}(\tau, k) = \frac{1}{6} \left(\frac{k}{\mathcal{H}} \right)^2 \int_0^\infty dv \int_{|1-v|}^{1+v} du \left(\frac{4v^2 - (1 + v^2 - u^2)^2}{4uv} \right)^2 \overline{I_{\text{RD}}^2(v, u, x)} \mathcal{P}_{\mathcal{R}}(kv) \mathcal{P}_{\mathcal{R}}(ku), \quad (2.20)$$

and in the late time limit $x \rightarrow \infty$, one gets

$$\overline{I_{\text{RD}}^2(v, u, x \rightarrow \infty)} = \frac{1}{2} \left(\frac{3(u^2 + v^2 - 3)}{4u^3 v^3 x} \right)^2 \left[\left(-4uv + (u^2 + v^2 - 3) \log \left| \frac{3 - (u+v)^2}{3 - (u-v)^2} \right| \right)^2 + \pi^2 (u^2 + v^2 - 3)^2 \Theta(u + v - \sqrt{3}) \right]. \quad (2.21)$$

Note that, in order to calculate the GWs energy density, one needs to compute a $2d$ integral with an involved integrand. This integral can be solved numerically, after changing to a new set of variables which make it easier to solve. To the best of our knowledge, the GWs spectral energy density has only been calculated completely analytically for very few cases, for instance, when the power spectrum $\mathcal{P}_{\mathcal{R}}$ is a delta function at smaller scales [52, 72]. In all other cases and in particular, in inflationary models when the power spectrum $\mathcal{P}_{\mathcal{R}}$ is calculated completely numerically, this integral can only be evaluated numerically to obtain the resulting GWs spectrum for various cases.

2.3 The present spectral energy density of GWs

In order to compare the predictions of a given scenario of GWs production with the sensitivities of present and future GWs detectors, one needs to calculate the GWs spectral energy

density at the present epoch. Since the energy density of GWs decays as radiation $\rho \sim a^{-4}$, we can calculate the fraction of energy density of GWs in terms of the current energy density of radiation $\Omega_{r,0}$ and $\Omega_{\text{GW}}(\tau_f, k)$ at a time τ_f during the RD era, before all the available degrees of freedom become non-relativistic. We define the effective energy density of GWs per logarithmic interval of k through

$$\rho_{\text{GW}}(\tau) \equiv \int d \ln k \rho_{\text{GW}}(\tau, k), \quad (2.22)$$

where we assume the homogeneity and isotropy of these GWs. We shall briefly comment on the anisotropy of GWs in the final section. The present value of $\Omega_{\text{GW}}(\tau_0, k)$ can be written as follows

$$\Omega_{\text{GW}}(\tau_0, k) = \frac{\rho_{\text{GW}}(\tau_0, k)}{\rho_{\text{GW}}(\tau_f, k)} \frac{\rho_r(\tau_f)}{\rho_r(\tau_0)} \frac{\rho_r(\tau_0)}{\rho_c} \Omega_{\text{GW}}(\tau_f, k). \quad (2.23)$$

Using the conservation of entropy, we obtain

$$\frac{\rho_{\text{GW}}(\tau_0, k)}{\rho_{\text{GW}}(\tau_f, k)} = \left(\frac{a_f}{a_0} \right)^4, \quad (2.24)$$

$$\frac{\rho_r(\tau_f)}{\rho_r(\tau_0)} = \frac{\frac{\pi^2}{30} g_{*,f} T_f^4}{\frac{\pi^2}{30} g_{*,0} T_0^4} = \left(\frac{g_{*,f}}{g_{*,0}} \right) \left(\frac{g_{*,s,0}}{g_{*,s,f}} \right)^{4/3} \left(\frac{a_0}{a_f} \right)^4, \quad (2.25)$$

$$\frac{\rho_r(\tau_0)}{\rho_c} = \Omega_{r,0}. \quad (2.26)$$

If there are no extra relativistic degrees of freedom (beyond SM) at $\tau = \tau_f$ and using entropy conservation, we find

$$c_f = \frac{g_{*,f}}{g_{*,0}} \left(\frac{g_{*,s,0}}{g_{*,s,f}} \right)^{4/3} \approx 0.4. \quad (2.27)$$

This allows us to write down the final expression for $\Omega_{\text{GW}}(\tau_0, k)$ as

$$\Omega_{\text{GW}}(\tau_0, k) h^2 \simeq 6.6 \times 10^{-7} \left(\frac{\Omega_{r,0} h^2}{4.0 \times 10^{-5}} \right) \left(\frac{k}{\mathcal{H}(\tau_f)} \right)^2 \overline{\mathcal{P}_h(\tau_f, k)}, \quad (2.28)$$

which can also be written in terms of frequency f using the following relation

$$f = \frac{k}{2\pi} = 1.5 \times 10^{-15} \left(\frac{k}{1 \text{ Mpc}^{-1}} \right) \text{ Hz}. \quad (2.29)$$

In order to compute $\Omega_{\text{GW}}(\tau_0, k)$, we need to perform the integral in equation (2.19) numerically. However, this integral can also be computed analytically for very few cases such as the case of a delta function power spectrum. As has been discussed earlier, it turns out to be very useful to make a change of variables as $d = (u - v)/\sqrt{3}$ and $s = (u + v)/\sqrt{3}$, we get

$$\begin{aligned} \Omega_{\text{GW}}(\tau_0, k) h^2 \simeq & 2.4 \times 10^{-5} \left(\frac{\Omega_{r,0} h^2}{4.0 \times 10^{-5}} \right) \left(\frac{k}{\mathcal{H}(\tau_f)} \right)^2 \int_{-\frac{1}{\sqrt{3}}}^{\frac{1}{\sqrt{3}}} dd \int_{\frac{1}{\sqrt{3}}}^{\infty} ds \left[\frac{(d^2 - 1/3)(s^2 - 1/3)}{s^2 - d^2} \right]^2 \\ & \times \mathcal{P}_{\mathcal{R}} \left(\frac{k\sqrt{3}}{2}(s + d) \right) \mathcal{P}_{\mathcal{R}} \left(\frac{k\sqrt{3}}{2}(s - d) \right) \left[\mathcal{I}_c^2(d, s) + \mathcal{I}_s^2(d, s) \right]. \end{aligned} \quad (2.30)$$

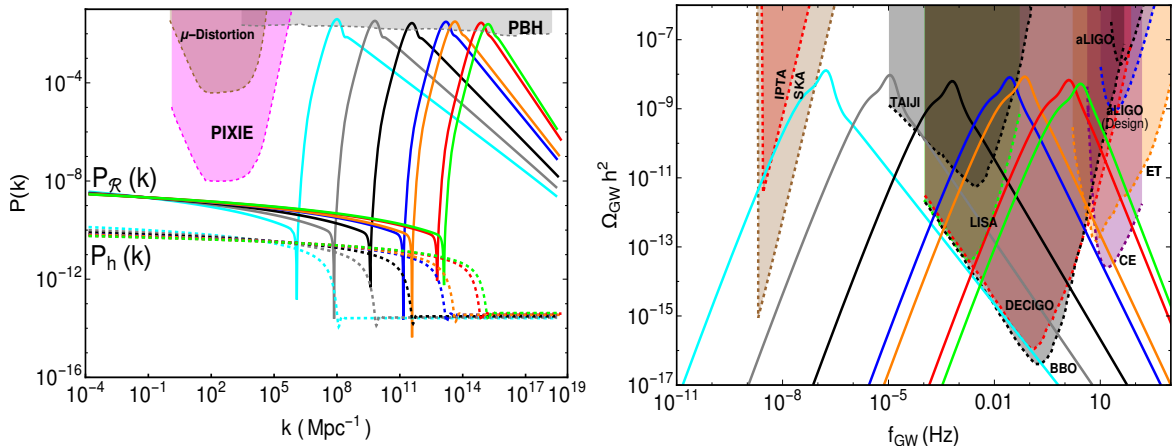


Figure (1) On the left, we plot the power spectra of primordial curvature perturbations $\mathcal{P}_{\mathcal{R}}$ (solid curves) and primordial tensor perturbations \mathcal{P}_h (dashed curves) for different parameters of the scenario that we had discussed in our earlier work [32]. All these spectra show a similar enhancement at smaller scales, required for the abundant PBHs production. Also, shown are the relevant constraints from CMB distortions and PBHs formation. On the right, we plot the spectral energy density of induced GWs corresponding to the spectra on the left. All the GWs spectra also show a similar behaviour. In particular, a bump in $\mathcal{P}_{\mathcal{R}}$ on small scales (large k) leads to a peak in $\Omega_{\text{GW}}h^2$ on larger frequencies which fall in the sensitivity regimes of various future space based GWs observatories such as LISA, TAIJI, DECIGO or BBO. The colour coding of different plots is consistent across the two figures.

This is the final expression we directly use in our numerical routine together with the analytical results for \mathcal{I}_c and \mathcal{I}_s in an appropriate limit which are given in the following compact form as [72]

$$\mathcal{I}_c(d, s) = -36\pi \frac{(s^2 + d^2 - 2)^2}{(s^2 - d^2)^3} \theta(s - 1), \quad (2.31)$$

$$\mathcal{I}_s(d, s) = -36 \frac{(s^2 + d^2 - 2)}{(s^2 - d^2)^2} \left[\frac{(s^2 + d^2 - 2)}{(s^2 - d^2)} \log \frac{(1 - d^2)}{|s^2 - 1|} + 2 \right]. \quad (2.32)$$

In our previous work [32], we had developed a numerical code to compute the PBHs mass fraction for inflationary models which allows violations of SR condition, needed for the enhancement of the power spectrum to produce sufficient mass fraction of PBHs. We have now extended that code by including a routine to also compute the induced GWs background in such models. In figure 1, we have plotted the power spectra of primordial curvature and tensor perturbations $\mathcal{P}_{\mathcal{R}}$ and \mathcal{P}_h for the scenario that we had discussed in our earlier work [32]. The power spectra $\mathcal{P}_{\mathcal{R}}$ correspond to different choices of parameters of the model which leads to different values of the spectral index n_s at the pivot scale. All these spectra show a similar enhancement $\mathcal{P}_{\mathcal{R}} \sim k^4$ at smaller scales, an interesting behaviour which has also been obtained using an analytical formalism [73, 74]. In the right panel of this figure, we have plotted the corresponding spectral energy density $\Omega_{\text{GW}}h^2$ of induced GWs, obtained by numerically integrating equation (2.30). We found that all the GWs spectra show a similar

behaviour, with a peak at a characteristic frequency which can be determined using equation (2.29). In particular, and as also expected, a bump in $\mathcal{P}_{\mathcal{R}}$ leads to a peak in $\Omega_{\text{GW}}h^2$ which fall in the sensitivity regimes of various future space based GWs observatories such as LISA, TAIJI, DECIGO or BBO. As we have found in our scenario, a wider power spectrum $\mathcal{P}_{\mathcal{R}}$ will result in a wider induced GWs spectra spanning a broader frequency range. This is interesting because the induced signal overlaps with the design sensitivity plots of different GWs observatories, particularly around the mHz - Hz range. In such a situation, there lies an interesting possibility to simultaneously detect these signals with different observatories and obtain stronger constraints on its origins in terms of the model parameters. It is also interesting to note that, for some cases in our model wherein the bump in the scalar power spectrum is located on rather larger scales (but still much smaller than CMB scales), the resulting induced GWs background can also be detected by an array of future IPTA/SKA detectors [75, 76].

Having computed the power spectrum of induced tensor perturbations, it is interesting and relevant to understand the extent of the induced tensor bispectrum in such models and analyse whether its imprints could possibly be detected by space based GWs observatories. Recently, it has been pointed out that the non-Gaussianity associated with the induced tensor bispectrum in some models can be large [53, 54] and it is imperative to think about the extent of this bispectrum in other inflationary models. Moreover, one can naively expect that all such models which induce a large stochastic GWs background due to the enhancement of primordial curvature perturbations will also generally induce a large tensor bispectrum at the time of GWs production i.e. some time after the horizon re-entry of different modes. However, it has been further emphasised that this peculiar non-Gaussian characteristic of the signal may not be observable unfortunately in any GWs detector at present. Since the detectors can only measure the superposition of such signals coming from many different directions in the sky and not just from one line of sight, such non-Gaussianities (or the phase correlations) would be further de-correlated by the propagation of GWs from different directions due to the inhomogeneities present from their generation epoch to today and thus, will not be observable [53].

2.4 The spectral tilt of the induced GWs spectrum

In this section, we try to provide an understanding of the spectral tilt before and after the peak of the GWs spectrum that we have numerically calculated for various cases of our scenario, as shown in figure 1. Let's assume that the power spectrum of curvature perturbations $\mathcal{P}_{\mathcal{R}}$ is peaked at some scale $k = k_p$. We shall closely follow the discussion of Refs. [77, 78] and compare our results with them. Since the leading contribution to the secondary GWs spectrum arises mainly from the enhanced power spectrum (relative to the CMB scales), we neglect the contribution arising from those very large scales and thus, $k_- < k < k_+$. This allows us to define a dimensionless parameter $\Delta = \frac{k_+ - k_-}{k_p}$ which quantifies the width of the power spectrum [77]. Note that, a narrow power spectrum corresponds to $\Delta \ll 1$. We are interested in the infrared behaviour of $\Omega_{\text{GW}}(k)$ in the regimes $k \ll k_-$ and $1 \ll k_-/k < k_+/k$. In this regime, one finds that the equation (2.20) reduces to

$$\Omega_{\text{GW}}(\tau, k) \propto \int_{\frac{k_-}{k}}^{\frac{k_+}{k}} dv \int_{u_1}^{u_2} du \left(\frac{4v^2 - (1 + v^2 - u^2)^2}{4uv} \right)^2 \frac{1}{I_{\text{RD}}^2(v, u, x)} \mathcal{P}_{\mathcal{R}}(kv) \mathcal{P}_{\mathcal{R}}(ku), \quad (2.33)$$

where $u_1 = \max\left(\frac{k_-}{k}, |1 - v|\right)$ and $u_2 = \min\left(\frac{k_+}{k}, 1 + v\right)$. Now, using the fact that the condition $k \ll k_-$ translates to $k/k_p \ll \Delta$, the above integral over v and u can be divided into three parts as

$$\Omega_{\text{GW}}(\tau, k) \propto \left[\int_{\frac{k_-}{k}}^{\frac{k_-}{k}+1} dv \int_{\frac{k_-}{k}}^{1+v} du + \int_{\frac{k_-}{k}+1}^{\frac{k_+}{k}-1} dv \int_{v-1}^{1+v} du + \int_{\frac{k_+}{k}-1}^{\frac{k_+}{k}} dv \int_{v-1}^{\frac{k_+}{k}} du \right] \times \left(\frac{4v^2 - (1 + v^2 - u^2)^2}{4uv} \right)^2 \overline{I_{\text{RD}}^2(v, u, x)} \mathcal{P}_{\mathcal{R}}(kv) \mathcal{P}_{\mathcal{R}}(ku). \quad (2.34)$$

Now using the regime $1 \ll k_-/k < k_+/k$, we find that the dominant contribution to the above integral comes from the second term only and the first and the third terms are much smaller. Since $v \in [k_-/k, k_+/k] \gg 1$ and also, $u \sim v$ in this case which simplifies the integral considerably and can be written in a final form as

$$\Omega_{\text{GW}}(\tau, k) = \frac{32}{81} \int_{\frac{k_-}{k}}^{\frac{k_+}{k}} dv \overline{I_{\text{RD}}^2(v, v)} \mathcal{P}_{\mathcal{R}}^2(kv). \quad (2.35)$$

Now, using the equation (2.21), we also find in this limit that

$$\overline{I_{\text{RD}}^2(v, v)} \simeq \frac{243}{64} \frac{1}{v^4} \ln^2\left(\frac{4v^2}{3}\right), \quad (2.36)$$

which finally leads to

$$\Omega_{\text{GW}}(\tau, k) \simeq \frac{3}{2} \int_{\frac{k_-}{k}}^{\frac{k_+}{k}} \frac{dv}{v^4} \ln^2\left(\frac{4v^2}{3}\right) \mathcal{P}_{\mathcal{R}}^2(kv). \quad (2.37)$$

We now need to solve this integral to obtain the tilt of the GWs power spectrum. If we define a new variable z as $1 + z = (k/k_p)v$, the above integral can be rewritten as

$$\begin{aligned} \Omega_{\text{GW}}(\tau, k) &\simeq \frac{3}{2} \left(\frac{k}{k_p}\right)^3 \int_{\frac{k_-}{k_p}-1}^{\frac{k_+}{k_p}-1} \frac{dz}{(1+z)^4} \ln^2 \left[\frac{4k_p^2}{3k^2} (1+z)^2 \right] \mathcal{P}_{\mathcal{R}}^2[k_p(1+z)], \quad (2.38) \\ &\simeq \frac{3}{2} \left(\frac{k}{k_p}\right)^3 \ln^2\left(\frac{4k_p^2}{3k^2}\right) \mathcal{P}_{\mathcal{R}}^2(k_p). \end{aligned}$$

The last line is the leading order result in Δ which also provides the tilt of the GWs spectra before the peak. In terms of the frequency f , we find that

$$\Omega_{\text{GW}}(\tau, f) \propto f^3 \ln^2\left(\frac{f_p}{f}\right)^2. \quad (2.39)$$

In the strict infrared limit $k \rightarrow 0$, one obtains $\Omega_{\text{GW}} \propto k^3 \propto f^3$ which has been discussed as a rather universal result in this limit [78]. We found that the logarithmic scaling matches very well with the GWs spectral density Ω_{GW} obtained numerically. We now look at the other regime *i.e.* $k \gg k_p$ and parametrise the power spectrum as $\mathcal{P}_{\mathcal{R}} \sim k^\beta$ for $k \gg k_p$. For

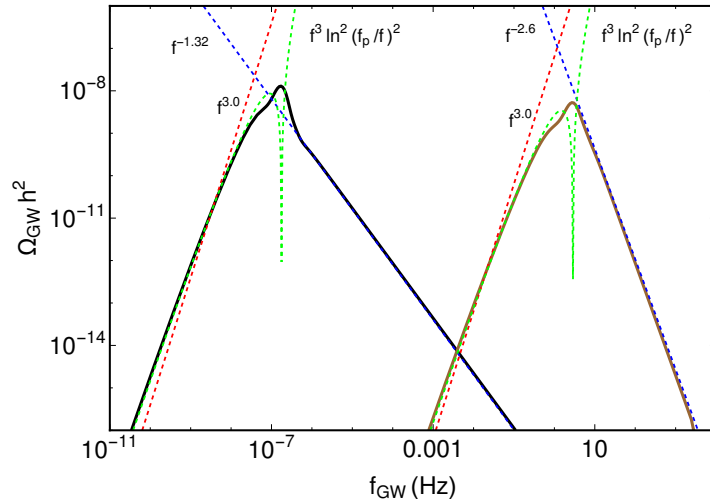


Figure (2) We plot the spectral energy density $\Omega_{\text{GW}} h^2$ of secondary GWs for two cases. To compare the tilt of the spectra before the peak, we also plot the infrared behaviour $\Omega_{\text{GW}}(f) \propto f^3$ (red dashed) as well as the logarithmic behaviour $\Omega_{\text{GW}}(f) \propto f^3 \ln^2(f_p/f)^2$ (green dashed). We find that the logarithmic behaviour matches very well with the exact GWs spectra obtained numerically in both the cases. Moreover, the tilt of the GWs spectra after the peak also matches quite well with the qualitative result $\Omega_{\text{GW}}(f) \propto f^{2\beta}$ (blue dashed). For these two cases with $\beta \simeq -0.66$ and -1.3 , we find that $2\beta \geq -4.0$, as discussed in the text.

this case, $v, u \ll 1$, the integrand of equation (2.20) drastically simplifies to $v^{(3-\beta)}$. Now if $\beta > -4$, we find that

$$\Omega_{\text{GW}}(k) \propto k^{2\beta} \int_{-\infty}^{\infty} dv F(v), \quad (2.40)$$

and therefore, $\Omega_{\text{GW}}(k) \propto k^{2\beta} \propto f^{2\beta}$ as the integration is independent of k . Similarly, for $\beta \leq -4$, again the leading contribution to the integral in equation (2.20) comes from the domain $k_p/k \leq (v, u) \ll 1$ and thus, we find that

$$\Omega_{\text{GW}}(k) \propto k^{2\beta} \int_{k_p/k}^{\sigma} dv v^{(3-\beta)}, \quad (2.41)$$

where the allowed range of σ is defined by $k_p/k \ll \sigma \ll 1$. After simplification, this leads to

$$\Omega_{\text{GW}}(k) \propto k^{(\beta-4)} \propto f^{(\beta-4)} \quad \text{for } \beta < -4, \quad (2.42)$$

and for the case of $\beta = -4$

$$\Omega_{\text{GW}}(k) \propto k^{(\beta-4)} \ln\left(\frac{k_p}{k}\right) \propto f^{(\beta-4)} \ln\left(\frac{f_p}{f}\right), \quad (2.43)$$

where f_p is the frequency associated with the peak in Ω_{GW} , as can also be derived from equation (2.29). This provides us a qualitative understanding of the tilt of the GWs spectrum before and after the peak [78–80].

In order to compare these qualitative and approximate results with the exact GWs spectra, in figure 2, we have plotted the spectral energy density of GWs for two cases. As discussed earlier, the slope of the GWs spectra before the peak is always given by $\Omega_{\text{GW}}(f) \propto f^3 \ln^2(f_p/f)^2$ which we plot on top of the exact spectra. We find that in both the cases, it matches very well with the exact result while the infrared scaling $\Omega_{\text{GW}}(f) \propto f^3$ is not such a good fit.

Now, to understand the slope of the scalar power spectrum after the peak, let's borrow our discussion of Section 4 and assume that after the peak at $N = N_0$, ϵ grows as $\epsilon \propto e^{\gamma N}$ where γ stays nearly constant upto the end of inflation which leads to

$$\ln\left(\frac{\epsilon(N_e)}{\epsilon(N_0)}\right) = \gamma(N_e - N_0). \quad (2.44)$$

Using the minimum bound as we obtain later in Section 4, $N_e - N_0 \geq 10.36$ [c.f. equation (4.6)] and using $\epsilon_0 = \epsilon(N_0) \simeq 10^{-9}$ as $\epsilon(N_e) = 1$ at the end of inflation, we get $\gamma \leq 2.0$. If we now assume that $P_{\mathcal{R}} \sim k^\beta$ after the peak and since $k \propto e^N$, using (4.1) we get $\beta = -\gamma$ and thus β follows the limit $\beta \geq -2.0$ and thus, the scaling of GWs spectrum is $\Omega_{\text{GW}}(f) \propto f^{2\beta}$ with $2\beta \geq -4.0$. This result is also in good agreement with [80], in appropriate limit. This provides us a very rough estimate of the GWs spectra after the peak. Although we have only plotted two GWs spectra in Figure 2 but we find that all our GWs spectra of Figure 1 do always satisfy the condition of $2\beta \geq -4.0$ which indicates that such bounds provide us extra information that is consistent with the exact numerical GWs spectra obtained in all the other cases.

3 Observing ultralight PBHs with Advanced LIGO

As we had mentioned in our earlier work [32], our scenario can produce PBHs in very different mass ranges and all these mass windows are constrained by a variety of observations. However, it turns out that there do not seem to be any observational constraints around the asteroid mass window and thus, PBHs could contribute to the total energy density of CDM around that window, as has been emphasised in the literature recently. It is well known that PBHs do evaporate due to Hawking radiation and the evaporation time scale is given by

$$t_{\text{ev}}(M) \sim \frac{G^2 M^3}{\hbar c^4} \sim 10^{63} \left(\frac{M}{M_\odot}\right)^3 \text{ yr}. \quad (3.1)$$

This implies that PBHs with mass $M \lesssim 10^{-18} M_\odot$ ($M \lesssim 10^{15}$ g) would be completely evaporated by today and thus can not contribute to the present density of the CDM in the universe [81, 82]. PBHs in the mass range $10^{-18} - 10^{-16} M_\odot$ would actually be evaporating at the present epoch and thus can induce an observable γ -ray background [83]. However, PBHs in the very low mass range would not contribute to the CDM at all and would also be completely evaporated by today. However, they might still induce a secondary GWs background which could, in principle, be detected by the future designs of the ground based GWs observatories.

It is interesting to note that, the three ‘‘peaks’’ *i.e.* the position of the peak in the power spectrum of curvature perturbations, the peak height in the PBHs mass distribution and the frequency of the peak of the GWs signal are related by [51, 53, 84]

$$\left(\frac{M_{\text{PBH}}}{10^{17} \text{ g}}\right)^{-1/2} \simeq \frac{k}{2 \times 10^{14} \text{ Mpc}^{-1}} = \frac{f}{0.3 \text{ Hz}}, \quad (3.2)$$

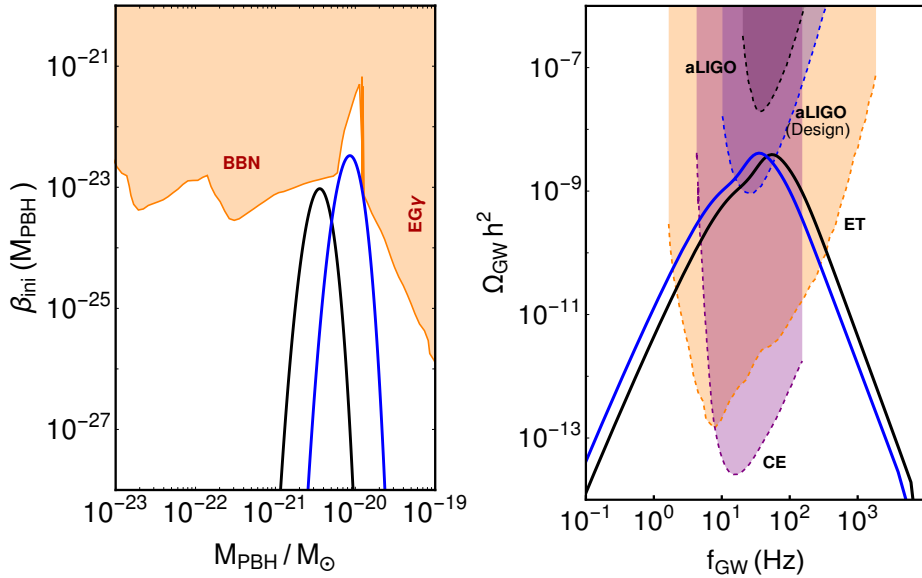


Figure (3) On the left, we plot the PBHs mass fraction at the formation epoch for two different cases, produced in our model [32] in the very low mass range corresponding to $M \sim 10^{-20} - 10^{-21} M_{\odot}$, as well as the observational constraints arising from big bang nucleosynthesis (BBN) and extragalactic γ -ray background. Such small mass PBHs would have been completely evaporated by today due to Hawking radiation. However, they will still induce an observable secondary GWs background in the higher frequency range which falls in the design sensitivity contours of the Advanced LIGO detector and therefore, can, in principle, be detected in future runs, as shown on the right panel.

which provides a qualitative understanding of the relation among M_{PBH} , k and f . This relation roughly indicates that a peak in the power spectrum of curvature perturbations at $k \simeq 2 \times 10^{14} \text{Mpc}^{-1}$ would generate a peak in the GWs spectrum at frequency $f \sim 0.3 \text{Hz}$. Moreover, as the sensitivity is maximum for LISA at $f \sim \text{mHz}$, the peak in $\mathcal{P}_{\mathcal{R}}$ should be around $k \sim 10^{12} \text{Mpc}^{-1}$ which is consistent with what is shown in figure 1. This scaling can further be used to roughly figure out what mass range of PBHs can possibly be probed by means of their secondary GWs signatures using the ground based detectors such as Advanced LIGO. The maximal sensitivity of the projected design of the Advanced LIGO detector corresponds to $f \sim 30 \text{Hz}$. A stochastic GWs signal around this frequency would correspond to very light PBHs with mass around $M_{\text{PBH}} \sim 10^{13} \text{g} \sim 10^{-20} M_{\odot}$. Evidently, from equation (3.1), all such PBHs would be completely evaporated through the emission of Hawking radiation from their formation to today and thus, can not constitute the observed abundance of CDM.

Note that, M_{PBH} here corresponds to the mass of a PBH at the formation epoch and disregards any further mass growth due to merging or accretion. Moreover, there exist various uncertainties associated with the numbers in this equation e.g. the efficiency factor γ which is defined as the ratio between the mass collapsing into a PBH and the total mass associated to that mode within the horizon. Its value is usually taken as $\gamma \sim 0.2$ [81, 85] but there could be some uncertainties associated with the PBH collapse. Often, the effects of critical collapse

are neglected wherein detailed numerical work has shown that the mass of PBHs formed after horizon reentry will depend on the amplitude of the overdensity δ . Secondly a slightly smaller value of the radiation energy density today will lead to an $\mathcal{O}(1)$ difference in this relation. Finally, a slight difference arises due to the value of g_* , the relativistic number of degrees of freedom in the thermal bath when the mode responsible for the PBH re-enters the horizon, although the dependence of M_{PBH} on g_* is weak. All these uncertainties could introduce a factor of $\mathcal{O}(10)$ in the final result so one should keep them in mind when comparing this relation with an exact numerical calculation, as is the case with our scenario.

In Figure 3, we have plotted the PBHs mass fraction at the formation epoch and the associated secondary GWs energy density for two different cases of our scenario [32]. The PBHs mass fraction at their formation epoch is also constrained to very small $\beta_{\text{ini}} \sim 10^{-23}$ from the BBN and extragalactic γ -ray background. However, as pointed out recently in [35] and we also observed it in our inflationary model, their induced stochastic GWs background fall right in the design sensitivity curves of a future configuration of Advanced LIGO detector and thus, can be potentially detected. Moreover, this GWs background also falls in the sensitivity contours of the proposed third generation ground based GWs detectors, Einstein Telescope (ET) and Cosmic Explorer (CE). Since this induced signal overlaps with all these three future GWs detectors, there lies again an interesting possibility of simultaneously detecting the signal with these GWs observatories and putting stringer constraints on its origin. Note that, the ground based GWs detectors such as LIGO and VIRGO have already detected the astrophysical GWs signals from a few systems of binary black holes and neutron stars with large masses and will detect many more in near future. However, the characteristic shape of the GWs spectrum in these two cases is very different and thus, can be easily disentangled. Recently, some prospects of probing such ultralight PBHs using their stochastic GWs signatures with the Advanced LIGO detector have been discussed in [86].

4 A lower bound on the PBHs mass for USR inflation

In Section 3, we had considered the observational imprints of ultralight PBHs in terms of their secondary GWs signatures and found that such GWs can in principle be detected with a future design run of the ground based Advanced LIGO detector. In this section, we shall try to understand how to derive a lower bound on the PBHs mass in the USR phase, both using an instantaneous transition as well as a smooth transition from the USR to the SR phase. We find that the lower bound obtained in both the scenarios are in agreement with each other. However, our bounds do not apply if there is an intermediate fast roll stage after the USR phase.

4.1 An instantaneous transition from USR to SR

In order to estimate the lower bound, we first need the estimation of minimum number of e-folds in the final SR phase followed by a USR phase. Assuming that the inflaton is rolling in the positive direction, $\phi_N = d\phi/dN$ is positive. Since ϕ_N always decreases during the USR phase, let's assume that at $N = N_0$, ϕ_N reaches its minimum value. This can also be considered the point after which the SR potential takes over and ϕ_N starts to increase again. Note that, at this point, $\phi_{NN} = 0$ and as the first SR parameter $\epsilon = \phi_N^2/2M_{\text{Pl}}^2$ is very small, the second SR parameter $\eta = \epsilon - (\phi_{NN}/\phi_N)$ is also very small and as a result, all the SR conditions are satisfied. Thus we can safely approximate the power spectrum of \mathcal{R}_k with the

SR result as

$$P_{\mathcal{R}}(k) \simeq \frac{1}{8\pi^2 M_{\text{Pl}}^2} \frac{H^2}{\epsilon_0}, \quad (4.1)$$

where $\epsilon_0 = \epsilon(N_0)$. Since we are considering an instantaneous transition from the USR to the SR phase, the smallest scale $k_0 = k(N_0)$ leaving the horizon would still be amplified and produce PBHs. Moreover, a significant mass fraction of PBHs requires an amplification of the power spectrum at PBHs scales as $P_{\mathcal{R}}(k) \sim 10^{-2}$, so equation (4.1) leads to

$$\epsilon_0 \simeq \frac{H^2}{M_{\text{Pl}}^2}. \quad (4.2)$$

Now, using the SR approximation during the horizon exit of the observable pivot scale k_p , we can safely use equation (4.1) to estimate the Hubble parameter H which stays nearly constant during inflation, as

$$\frac{H^2}{M_{\text{Pl}}^2} \sim 10^{-9}, \quad (4.3)$$

where we have used $P_{\mathcal{R}}(k_p) \sim 2.1 \times 10^{-9}$ and $\epsilon_p \sim 10^{-2}$ using $n_s(k_p) \simeq 0.965$. Now using (4.2) and (4.3), we can estimate the minimum value of ϵ_0 as $\epsilon_0 \sim 10^{-9}$ and the corresponding minimum value of $|\phi_{N_0}| \simeq \sqrt{2} \times 10^{-4.5}$. Using this estimation, we want to understand the minimum number of e-folds necessary from $N = N_0$ to the end of inflation at $N = N_e$, where $\epsilon(N_e) = 1$ or $\phi_{N_e} = \sqrt{2}$ must be satisfied. For this calculation, we shall assume that SR conditions are not violated again between the end of USR to the end of inflation and thus, the two conditions must be satisfied, $\epsilon \ll 1$ and $|\eta| \leq 1$. This leads to the following inequality

$$-1 \leq \frac{\phi_{NN}}{\phi_N} \leq 1 \quad \text{or} \quad \left| \frac{\phi_{NN}}{\phi_N} \right| \leq 1. \quad (4.4)$$

If we assume $\phi_{NN}/\phi_N = c(N)$, and solve it with the initial condition $\phi_N(N = N_0) = \phi_{N_0}$, we obtain

$$\log \left| \frac{\phi_N}{\phi_{N_0}} \right| = \int_{N_0}^{N_e} c(N) dN \quad (4.5)$$

Now using (4.4), $|c(N)| \leq 1$, so the minimum number of e-folds between N_0 to the end of inflation N_e ($\phi_{N_e} = \sqrt{2}$) is constrained as;

$$\Delta N = N_e - N_0 \geq \log \left| \frac{\sqrt{2}}{\phi_{N_0}} \right|. \quad (4.6)$$

Using our previous estimation $|\phi_{N_0}| \simeq \sqrt{2} \times 10^{-4.5}$, we get $\Delta N \geq 10.36$ which is roughly the duration of the final SR phase before the end of inflation.

4.2 A smooth transition from USR to SR

Our previous estimation of the minimum number of e-folds was independent of the form of the potential and we only assumed an instantaneous transition from the USR to SR phase. To extend our analysis for a smooth transition from USR to SR, we need to consider the

potential around $\phi(N_0) \equiv \phi_0$. Since USR phase is on a flat part of potential, we can effectively approximate the potential around ϕ_0 , with first few terms of the Taylor's expansion as

$$V(\phi) = b_0 + b_1(\phi - \phi_0) + b_2(\phi - \phi_0)^2 + \dots \quad (4.7)$$

In the vicinity of the USR phase, we can neglect ϕ_N^2 term and assume the Hubble parameter to be constant as $H(N) \simeq \sqrt{V(\phi_0)}/3 = \sqrt{b_0}/3$. This reduces the equation of motion for ϕ to

$$\phi_{NN} + 3\phi_N + \frac{1}{H^2} \frac{dV}{d\phi} = 0. \quad (4.8)$$

Now, using the initial condition that at $N = N_0$ inflation field value is ϕ_0 and the minima of ϕ_N is reached *i.e.* $\phi_{NN} = 0$, we obtain the dynamics of ϕ as [80]

$$\phi(N) = \phi_0 - \frac{b_1}{2b_2} + \frac{1}{4\alpha b_2} \times \left[\left(\alpha b_1 + \frac{4b_1 b_2}{3H} - 3b_1 H \right) e^{-\frac{(\alpha+3H)(N-N_0)}{2H}} + \left(\alpha b_1 - \frac{4b_1 b_2}{3H} + 3b_1 H \right) e^{\frac{(\alpha-3H)(N-N_0)}{2H}} \right],$$

where $\alpha = \sqrt{3b_0 - 8b_2}$. Assuming that the inflaton is rolling in the positive direction, at the minima, ϕ_N must be positive, to have a finite duration of the USR phase. So we need

$$\phi_N(N_0) = -\frac{b_1}{b_0} > 0 \quad \text{and} \quad \phi_{NNN}(N_0) = \frac{(6b_1 b_2)}{b_0^2} > 0. \quad (4.9)$$

These conditions constrain the possible value of potential parameters; $b_1 < 0$ and $b_2 < 0$. Using these, we can now express ϕ_N as a function of a single positive parameter b_6 as

$$\frac{\phi_N(N)}{\phi_N(N_0)} = \frac{\sqrt{3}}{b_6} e^{-3\Delta N/2} \sinh\left(\frac{\sqrt{3}}{2} b_6 \Delta N\right) + e^{-3\Delta N/2} \cosh\left(\frac{\sqrt{3}}{2} b_6 \Delta N\right), \quad (4.10)$$

where $b_6 = \sqrt{3b_0 - 8b_2}/\sqrt{b_0}$ and $\Delta N = N - N_0$. To avoid eternal inflation, we need $b_2 < 0$, so the minimum value of b_6 must be greater than $\sqrt{3}$. Now we want to estimate the number of e-folds from the peak in the power spectra to the point where the SR potential takes over completely (let's say at $N = N_s$). Our assumption is that this transition to SR must happen while $|\eta| \leq 1$ which then leads to

$$\epsilon(\Delta N) = 10^{-9} \left(\frac{\phi_N(\Delta N)}{\phi_N(N_0)} \right)^2, \quad (4.11)$$

$$\eta(\Delta N) = \epsilon(\Delta N) - \frac{\phi_{NN}(\Delta N)}{\phi_N(\Delta N)} = \epsilon(\Delta N) + \frac{9 - 3b_6^2}{2\sqrt{3} b_6 \coth\left(\frac{\sqrt{3}}{2} b_6 \Delta N\right) + 6}. \quad (4.12)$$

When the minima of ϕ_N is reached, $\phi_{NN} = 0$ and ϵ is very small ($\epsilon \sim 10^{-9}$) so very close to $N = N_0$, η crosses zero. Just after this crossing, ϕ_{NN} starts to increase and achieves a positive value which leads to an increase in ϕ_N as well. Very quickly, the ratio ϕ_{NN}/ϕ_N saturates, which is the second term of η with a negative sign, as in (4.12). It is interesting to note, that depending on the value of b_6 , this term saturates to a negative asymptotic value $\eta_{\text{asym}} = \frac{9-3b_6^2}{2\sqrt{3}b_6+6}$. Evidently, this saturation indicates the end of the transition phase. After this point, the further dynamics must be completely described by the SR potential. If this

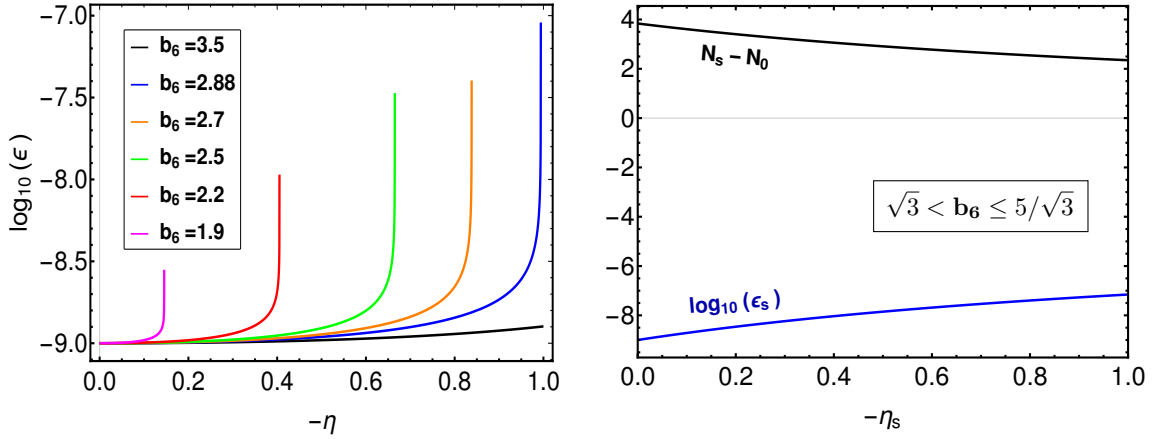


Figure (4) On the left, we have plotted the growing behaviour of ϵ before the transition, as obtained in equation (4.15). It is evident that for all values of b_6 in the range $\sqrt{3} < b_6 \leq 5/\sqrt{3}$, η saturates to a constant value, greater than -1 . On the right, the largest value of ϵ_s and the corresponding number of e-folds whenever η reaches its asymptotic value η_s .

saturation value $\eta_{\text{asym}} \leq -1$, the dynamics deviates from SR before the transition and enters a fast roll phase. We shall assume that there is no intermediate fast roll phase between USR and SR and consider only values of b_6 which ensures the transition to SR before $\eta \simeq -1$. Thus solving for $\phi_{NN}/\phi_N = 1$, we obtain

$$N(b_6) = \frac{2}{\sqrt{3} b_6} \coth^{-1} \left(\frac{\sqrt{3} (b_6^2 - 5)}{2b_6} \right). \quad (4.13)$$

In our case, b_6 is already constrained as $b_6 > \sqrt{3}$, the above equation further limits the value of b_6 to be less than $5/\sqrt{3}$ so we finally have $\sqrt{3} < b_6 \leq 5/\sqrt{3}$.

Now we want to understand what can be the maximum value of ϵ_s or ϕ_{N_s} during this transition and how many e-folds are spent to reach the transition. If we solve $\eta = -c$ for $0 < c < 1$, from (4.12) we get

$$N_c(b_6) = \frac{2}{\sqrt{3} b_6} \coth^{-1} \left(\frac{\sqrt{3} (b_6^2 - 2c - 3)}{2b_6 c} \right). \quad (4.14)$$

Upon using (4.14), at $N = N_c$ we can find ϵ as a function of b_6 as

$$\epsilon(b_6) = 3 \times 10^{-9} \frac{(b_6^2 - 3)}{3b_6^2 - (2c + 3)^2} \exp \left[-\frac{2\sqrt{3}}{b_6} \coth^{-1} \left(\frac{\sqrt{3} (b_6^2 - 2c - 3)}{2b_6 c} \right) \right] \quad (4.15)$$

This value of ϵ is plotted in figure 4 (on the left) and from this plot, we can clearly see that for every b_6 in the range $\sqrt{3} < b_6 \leq 5/\sqrt{3}$, η saturates to a constant value, $\eta > -1$. We can consider this saturation as the beginning of the SR phase and we need to use the value of ϵ during this saturation as the starting value of ϵ_s for the SR phase. Solving for $\phi_{NN}/\phi_N = -\eta_{\text{asym}} + \xi$ where ξ is negative and much smaller than η_{asym} , we can get the value of e-fold number where η reaches its asymptotic value and the value of ϵ_s , as plotted

on the right in figure 4. It is evident from these plots that $b_6 = 5/\sqrt{3}$ leads to the highest value of $\epsilon_s \simeq 7.0 \times 10^{-8}$ and the lowest value of $N_s - N_0 \simeq 2.34721$. This also corresponds to the quickest transition and largest possible transition value of $|\eta_s|$ whereas $b_6 \rightarrow \sqrt{3}$ leads to the lowest value of $\epsilon_s \simeq 1.0 \times 10^{-9}$ and largest value of $N_s - N_0 \simeq 3.83$.

Finally, the above values of ϵ_s can be translated to the bound on the number of e-folds using (4.6) and thus, we can calculate the total number of e-folds, before and after the SR transition for both the cases as

1. For $b_6 = 5/\sqrt{3}$, $\Delta N_{min} \simeq 2.35 + 8.23 = 10.58$
2. For $b_6 \rightarrow \sqrt{3}$, $\Delta N_{min} \simeq 3.83 + 10.36 = 14.19$

Thus, it is evident that for a smooth transition, even quickest possible transition takes more number of e-folds than our estimation in the previous section wherein we considered an instantaneous transition in a rather model independent manner.

4.3 Estimation of the lower bound on the PBHs mass

In order to estimate a lower bound on the PBHs mass from the USR phase, we first need to calculate the total number of e-folds from the horizon exit of the pivot scale $k_p = 0.05 \text{ Mpc}^{-1}$ to the end of inflation. In a RD universe, $a \propto t^{1/2}$, $H \propto t^{-1}$ and $k = aH \propto t^{-1/2} \propto H^{1/2}$, thus if a comoving wavenumber k re-enters the horizon during the RD epoch, we can relate it with the comoving mode k_{eq} of matter-radiation equality using the Hubble parameter during re-entry as

$$\frac{k}{k_{eq}} = \left(\frac{H}{H_{eq}} \right)^{1/2}. \quad (4.16)$$

Upon using $\rho_{eq} = 3H_{eq}^2 M_{Pl}^2$, H_{eq} can be related to the present Hubble parameter as

$$\rho_{eq} = 2\Omega_{r,0}\rho_c(1+z_{eq})^4 = 6\Omega_{r,0}H_0^2 M_{Pl}^2(1+z_{eq})^4, \quad (4.17)$$

$$H_{eq} \simeq \sqrt{\Omega_{r,0}} H_0(1+z_{eq})^2. \quad (4.18)$$

Taking $\Omega_{r,0} \simeq 8 \times 10^{-5}$, $z_{eq} \simeq 3400$ and $H_0 \simeq 2 \times 10^{-4} \text{ Mpc}^{-1}$, we find $H_{eq} \simeq 20.7 \text{ Mpc}^{-1}$. Note that, we are calculating H_{eq} by only taking into account the radiation energy density at the matter-radiation equality. Now at the pivot scale, we know both the amplitude and the tilt of the primordial spectrum from Planck so using (4.1), we can calculate H_{inf} during inflation which we assume to stay nearly constant up to the end of inflation which, for instantaneous reheating, is same as with the beginning of the RD epoch so $H_{inf} \simeq H_e \simeq H_r$ which is given by

$$H_e \simeq H_r \simeq (8\pi^2 M_{Pl}^2 P_{\mathcal{R}}(k)\epsilon)^{1/2}. \quad (4.19)$$

With this and (4.16), we can now calculate the comoving mode entering at the very beginning of the RD epoch, $k_r = a_r H_r$ as

$$k_r \simeq \frac{k_{eq}}{\sqrt{H_{eq}}} (8\pi^2 M_{Pl}^2 P_{\mathcal{R}}(k)\epsilon)^{1/4}. \quad (4.20)$$

Taking $k_{eq} \simeq 0.01 \text{ Mpc}^{-1}$ and $P_{\mathcal{R}}(k) \simeq 2.1 \times 10^{-9}$ at $k = k_p$, we find

$$k_r \simeq 1.94 \times 10^{24} \epsilon^{1/4} \text{ Mpc}^{-1}. \quad (4.21)$$

For the case of an instantaneous reheating, we can finally estimate the total number of e-folds from the horizon exit of the pivot scale to the end of inflation

$$N_e - N_p = \ln \left(\frac{k_r}{k_p} \right) \simeq 58.92 + \frac{1}{4} \ln \epsilon. \quad (4.22)$$

Using observational constraints on the value of $n_s \simeq 0.965$ at the pivot scale, we can roughly estimate $\epsilon \leq 10^{-2}$ which then limits $N_e - N_p \lesssim 57.77$. This is, of course, consistent with the results from [87] wherein the total number of e-folds from the horizon exit of the present horizon ($k_{\text{hor}} \simeq 2 \times 10^{-4} \text{ Mpc}^{-1}$) to the end of inflation is constrained to be $\Delta N_{\text{tot}} \simeq 63.3$.

We now want to estimate the maximum number of e-folds from the horizon crossing of k_p to the minima of ϕ_N at $N = N_0$ which we can translate to the smallest scale becoming super-horizon before the onset of the final SR phase. Assuming the Hubble parameter H to be nearly constant and $k_p = a(N_p)H = a_i e^{N_p} H$ where a_i is the scale factor at the beginning of inflation, using (4.6) and (4.22), we get

$$N_0 - N_p \simeq 57.77 - 10.36 = 47.41. \quad (4.23)$$

This corresponds to a scale $k_{\text{PBH}} = \sigma a(N_0)H$, which becomes super-horizon around $N = N_0$. Here $\sigma \ll 1$ is taken to ensure that super-horizon condition is satisfied

$$k_{\text{max}} = \sigma k_p e^{N_0 - N_p} \approx 1.94 \times 10^{19} \sigma \text{ Mpc}^{-1}, \quad (4.24)$$

thus the smallest possible comoving length scale associated with a PBH peak corresponds to k_{max} , or $k_{\text{PBH}} \leq k_{\text{max}}$. Now we can use the relation between the mass of PBHs and the frequency of second order induced GWs as in equation (3.2) to translate the upper limit on k in the above equation to a lower limit on the PBH mass, M_{PBH} and an upper limit on the frequency of corresponding second order GWs, f as

$$M_{\text{PBH}} \geq 6.14 \times 10^{-27} \sigma^{-2} M_{\odot} \quad (4.25)$$

$$f \leq 2.91 \times 10^4 \sigma \text{ Hz} \quad (4.26)$$

Now if we take a very conservative limit on the factor σ as $\sigma \leq 10^{-2}$, lowest possible value of PBH mass and the highest value of the second order GWs frequency turn out to be $M_{\text{PBH}} \geq 6.14 \times 10^{-23} M_{\odot}$ and $f \leq 2.91 \times 10^2 \text{ Hz}$, respectively. Interestingly these constraints just cover the Advanced LIGO frequency range so future runs of Advanced LIGO can be used to detect the existence of PBHs from USR models, as we have already discussed in detail in Section 3.

Recently, it has also been discussed in the literature that during their formation, the abundance of PBHs with masses $M < 10^9 \text{ g} \sim 5 \times 10^{-25} M_{\odot}$ are essentially not constrained so they can constitute the dominant component of energy density (since they behave as matter) and drive the dynamics of the universe for a brief period of time before their evaporation due to Hawking radiation [88]. However our analysis and results of these sections suggest that USR models of inflation can not possibly produce such ultra low mass PBHs to dominate the energy density of universe for even a short period of time. Thus one has to resort to a different mechanism of PBHs production to discuss those possibilities. It may be interesting to see if an intermediate fast roll phase can produce such ultra low mass PBHs which can dominate for a short while before their evaporation.

5 Imprints of reheating on the secondary GWs spectrum and the lower mass bound

In this section, we shall study the effects of a reheating stage after the end of inflation on the resulting secondary background of GWs. Without writing down explicit couplings of the inflaton to other fields and going into deeper details of the reheating epoch, one can still capture broad imprints of the reheating stage by parametrising it using two parameters N_{reh} and w_{reh} where N_{reh} is the number of e-folds during reheating and w_{reh} is the effective equation of state parameter during reheating. As we had discussed in our previous work [32], a non-instantaneous reheating stage alters the mapping of different length scales from their horizon exit to re-entry thereby affecting the normalisation of the scalar power spectra at the pivot scale and therefore, the mass fraction of PBHs that these scales collapse to form upon their horizon re-entry. In [32], we found that this leads to a shift in the scalar power spectra without affecting its overall shape. Since the secondary GWs background is calculated using the second order effects arising from the curvature perturbations, we find that the induced GWs background is also affected in a similar manner.

Note that, the time evolution of second order GWs is considerably different from the time evolution of the first order GWs as discussed in [47]. If we consider a prolonged epoch of matter dominated reheating phase, during matter domination the sub horizon modes of the first order GWs decay but second order GWs do not decay, as the source term arising from first order scalar perturbation is constant during matter domination. During the transition to the RD phase, the gravitational potential of the relevant modes shall show an oscillatory behaviour (due to the transfer function) and decay quickly [88]. Note that, the leading order contribution to stochastic GWs comes from the modes around the peak in the power spectra which are super horizon during the reheating phase. In this case, the subsequent evolution of the gravitational potential for relevant modes after the generation of GWs at horizon entry shall follow the transfer function for the RD universe. As a result, the change in primordial power spectra $\mathcal{P}_{\mathcal{R}}$ due to a non-zero duration of the reheating phase [32] shall also be reflected in the corresponding secondary GWs spectra.

All the modes which re-enter the horizon during the RD epoch will be affected by the reheating epoch. In order to quantify this effect, let's recall the following relation between the scale factor at different epochs

$$\frac{a_i}{a_0} = \frac{a_i}{a_e} \frac{a_e}{a_{\text{reh}}} \frac{a_{\text{reh}}}{a_0}, \quad (5.1)$$

with

$$\frac{a_i}{a_e} = e^{-N}, \quad \frac{a_e}{a_{\text{reh}}} = e^{-N_{\text{reh}}}, \quad \frac{a_{\text{reh}}}{a_0} = \frac{a_r}{a_0}. \quad (5.2)$$

where N denotes the number of e-folds during inflation and the end of reheating coincides with the onset of RD epoch. Assuming that the reheating epoch is characterised by an equation of state parameter $w_{\text{reh}} = p_{\text{reh}}/\rho_{\text{reh}}$, we find that $\rho_{\text{reh}} = \rho_e e^{-3N_{\text{reh}}(1+w_{\text{reh}})}$. Note that, instantaneous reheating corresponds to $N_{\text{reh}} = 0$ and $w_{\text{reh}} = 1/3$. We shall discuss four different scenarios of reheating corresponding to different values of N_{reh} and w_{reh} . Since the duration of the reheating stage can not be very long, we restrict ourselves to the parameter range $0 \leq N_{\text{reh}} \leq 10$ and $0 \leq w_{\text{reh}} \leq 1/3$. In figure 5, we have plotted the power spectra $\mathcal{P}_{\mathcal{R}}$ (solid curves) and \mathcal{P}_h (dashed curves) for our model corresponding to four different reheating histories. As we had shown in our earlier work [32], the power spectra of curvature perturbations show a shift in the peak for these different reheating scenarios. The primordial

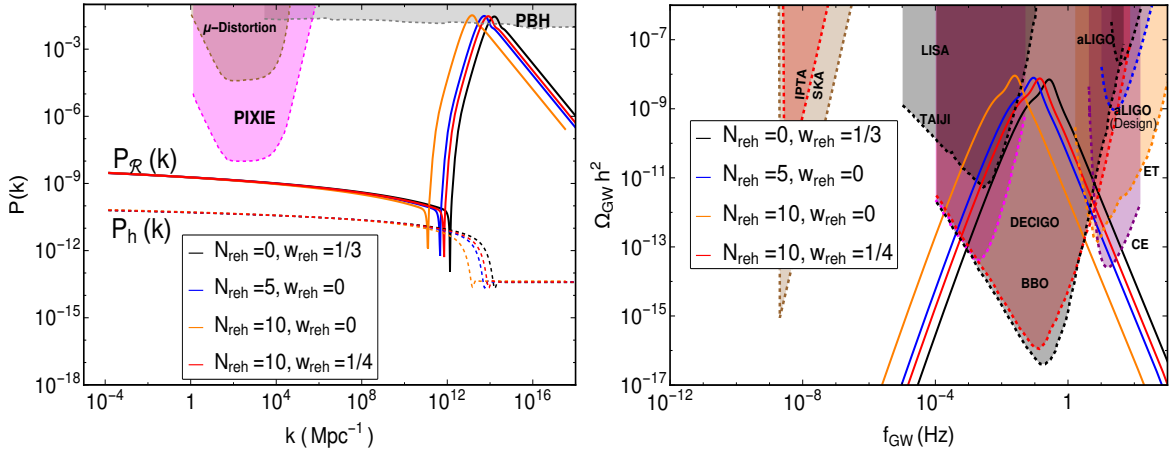


Figure (5) On the left, we plot the power spectra $\mathcal{P}_{\mathcal{R}}$ (solid curves) and \mathcal{P}_h (dashed curves) for our model corresponding to different reheating histories as displayed in the inset. Also, shown are the relevant constraints from CMB distortions and PBHs formation. The scalar spectra show a shift in the peak for the four different reheating scenarios that we have considered. The primordial tensor spectra for these cases also show a similar trend. On the right, we plot the induced GWs energy density corresponding to the spectra on the left. As the bump in $\mathcal{P}_{\mathcal{R}}$ shifts to smaller k , the peak of $\Omega_{\text{GW}} h^2$ shifts to smaller frequencies. Notably, the induced GWs background can be simultaneously observed by different detectors. The colour coding of different plots is consistent across the two figures.

tensor spectra also show a similar trend. On the right, we plot the induced GWs energy density corresponding to the spectra on the left for the same reheating scenarios which also show a similar shift as the reheating parameters are changed. As expected, the peak of $\Omega_{\text{GW}} h^2$ shifts to smaller frequencies as the bump in $\mathcal{P}_{\mathcal{R}}$ shifts to smaller k since $k \propto 1/f$. In particular, the effects due to a prolonged matter dominated reheating epoch i.e. $w_{\text{reh}} = 0$ and $N_{\text{reh}} = 10$ are significant. We conclude that as the GWs spectra are sensitive to reheating history, future space based GWs observatories can, in principle, probe and constrain the details of the reheating epoch of the early universe.

Following the same arguments as in the previous section, for non-instantaneous reheating epoch, equation (4.23) modifies to

$$N_0 - N_p \simeq 47.41 - \frac{1}{4} N_{\text{reh}} (1 - 3w_{\text{reh}}), \quad (5.3)$$

which implies that

$$k_{\text{max}} \simeq 1.94 \times 10^{19} \sigma e^{-\frac{1}{4} N_{\text{reh}} (1 - 3w_{\text{reh}})} \text{Mpc}^{-1}. \quad (5.4)$$

Since the maximum value of k shifts to an even lower value, both the lower bound on the PBHs mass and the upper bound on the GWs frequency become stronger and are given by

$$M_{\text{PBH}} \geq 6.14 \times 10^{-27} \sigma^{-2} e^{\frac{1}{2} N_{\text{reh}} (1 - 3w_{\text{reh}})} M_{\odot}, \quad (5.5)$$

$$f \leq 2.91 \times 10^4 \sigma e^{-\frac{1}{4} N_{\text{reh}} (1 - 3w_{\text{reh}})} \text{Hz}. \quad (5.6)$$

For $\sigma \leq 10^{-2}$, $w_{\text{reh}} = 0$ and $N_{\text{reh}} = 10$, these bounds translate to $M_{\text{PBH}} \geq 9.09 \times 10^{-21} M_{\odot}$ and $f \leq 23.94 \text{Hz}$. So evidently the lower bounds calculated in the previous section become even stronger in the presence of a non-zero duration of the reheating phase.

It is well known that the epoch of preheating/reheating after the end of inflation can also produce GWs. In particular, preheating can lead to resonant production of GWs [89]. However, we shall not discuss that very interesting aspect here. Moreover, the total number of relativistic degrees of freedom N_{eff} also affects the GWs background and its effects has been studied mostly for the primordial GWs background generated from the vacuum fluctuation during inflation. Since the secondary background of GWs generated from large primordial curvature perturbations in all models is primarily produced at the time of horizon re-entry of Fourier modes during the RD epoch and N_{eff} does not change significantly after RD epoch within the Standard model, we strongly believe that this induced GWs background will not be affected. However, in scenarios wherein an extra dark radiation component is present at that epoch or in scenarios beyond the standard model of particle physics, N_{eff} could change and may lead to a noticeable imprint on the induced GWs background.

6 Conclusions and discussions

In this paper, we have studied the induced stochastic GWs background from the enhancement of primordial curvature perturbations at smaller scales. An enhancement of the power spectrum is a very generic feature of all the inflationary models allowing the violation of slow roll conditions [90–92]. In our previous work [32], we had presented an inflationary scenario with a polynomial potential containing an inflection point which can generate PBHs in different mass windows with a nearly monochromatic mass fraction. In particular, PBHs generated in the asteroid mass window are very interesting as first, they can contribute to the entire CDM in the universe and second, the induced GWs have a characteristic peak around the mHz frequency band which can be probed by the future space based GWs observatories such as LISA, DECIGO or BBO. We have also shown that the secondary GWs induced by more massive PBHs which will be peaked in the lower frequency range can be probed by IPTA/SKA observations. Interestingly, in this scenario, we also notice that very light PBHs which may completely evaporate by today and would not contribute to the dark matter at all, will also generate a stochastic background of GWs that may be observed from a future design of the ground based Advanced LIGO detector. Using a model independent approach, we have also obtained a lower bound on the PBHs mass by only assuming an instantaneous and a smooth transition from the USR to the SR phase. We also investigate the effects of reheating on the secondary GWs spectrum and find that an epoch of a non-instantaneous reheating can cause a shift in the GWs spectrum to larger frequencies, thereby making it accessible to the reach of different GWs observatories. The lower mass bound of PBHs also become stronger in the case of a non-instantaneous reheating epoch.

In general, all cosmological sources of GWs typically produce stochastic backgrounds of GWs with a frequency roughly related to the size of the comoving Hubble horizon at the time of their production. It is worth pointing out that the entire mechanism of PBHs generation from scalar field inflationary models¹ leads to different characteristic backgrounds of GWs which can be distinguished based on their spectral energy density and frequency range.

- Primordial GWs background from vacuum tensor fluctuations characterised by the tensor to scalar ratio r . This background is typically very small and highly redshifted

¹It is well known that dynamical gauge fields during inflation provide very rich and interesting phenomenology [93–99]. In models wherein PBHs are produced due to the amplification of gauge fields, there exists another primordial contribution to tensor perturbations sourced directly by enhanced gauge fields during inflation [100, 101].

since its generation during inflation thus can not be directly detected with present or future GWs observatories

- Secondary GWs background sourced by the enhanced scalar perturbations in models of PBHs formation. Such GWs production is maximized when the scalar modes re-enter the horizon during the RD era but decay inside the horizon. This induced contribution typically has a broad peak in the spectra energy density which can be probed with various ground and space based GWs detectors.
- The GWs produced by the mergers of PBHs binaries since formation until today [102, 103]. The frequency of this GWs signal is in the Hz - kHz regime which falls in the sensitivity band of ground based detectors such as LIGO and future runs such as O5 of Advanced LIGO. Perhaps, the binary black hole systems detected by LIGO are PBHs binaries. The most recently detected merger event [104] also points out to a strong possibility of these intermediate mass black hole's origin being primordial [105].
- The GWs are also produced due to the graviton emission from Hawking evaporation of PBHs [88]. The emitted GWs from tiny PBHs with high Hawking temperature typically have very high frequency and thus, quite far from the reach of near future GW observatories.

Recently, it has been discussed whether the spectral energy density of induced GWs in the RD era from second order scalar perturbations is gauge invariant. In principle, a physical observable today should not depend on the choice of the gauge in which the calculations are carried out. There have been a few papers discussing this issue lately [106–110] and all of them seem to present different conclusions. All these papers have computed the spectral energy density of induced gravitational waves in the Newtonian, comoving and the uniform curvature gauges. In [106], it was noticed that there are huge differences in the final result between the Newtonian and the comoving gauge while the uniform curvature gauge gives the same result as the Newtonian gauge. However, in [107–109], it was claimed that the induced GWs today are gauge invariant while ref. [110] claims that the result is identical in four different gauges but still different than other gauges. In summary, the issue of gauge invariance for second order GWs is not yet completely settled and requires further investigation.

It has been pointed out recently that anisotropies in the GWs background are an interesting observable that can be used to distinguish among different GWs production mechanisms [111, 112]. These anisotropies refer to a change in the spectral energy density of observed GWs as a function of direction in the sky and can be imprinted both at the generation epoch as well as due to their propagation through the perturbed universe from the formation epoch to today. These anisotropies are similar to the CMB anisotropies and can be computed using a Boltzmann approach taking into account both the scalar and tensor perturbations [113–115]. Recently, the effects of primordial curvature perturbations on GWs propagation over cosmic distances have been calculated and it was shown that the resulting deformations of the GWs background can be significant for extremely peaked GWs spectra [116]. It will be very interesting to study these anisotropies in the case of scalar induced GWs background and see if they provide further insights into the mechanism of PBHs formation and the associated secondary GWs background produced in the early universe [117].

Detecting very high frequency GWs is going to be a big challenge for future detectors as high frequency poses severe complications for interferometric observatories. An interesting thought in this context is based on an indirect detection of these high frequency GWs by

means of their conversion into electromagnetic (EM) radiation (gravitons \rightarrow photons) in the presence of a cosmological background magnetic field. This effect is often called the inverse Gertsenshtein effect [118, 119]. It has been discussed that relic gravitons emitted by PBHs prior to Big Bang Nucleosynthesis would transform to an almost isotropic background of electromagnetic radiation due to their conversion [120–122]. This can be calculated at the recombination epoch and during the subsequent evolution of the universe. Since the produced EM radiation is concentrated in the X-ray part of the spectrum, this contribution could be observable and even dominate the cosmic X-ray background. We plan to investigate all such interesting issues in future.

Note added: While completing this paper, the NANOGrav collaboration put out a paper in the arxiv using their 12.5-year pulsar timing data set. They found a strong evidence of an isotropic stochastic GWs background around the nano-Hz frequency range [123]. It will be very interesting to see if massive PBHs produced during inflation in realistic models can provide an explanation for the observed NANOGrav signal [124, 125].

Acknowledgment

RKJ would like to thank Chris Byrnes for useful discussions and pointing to relevant references during COSMO19. The financial support from the new faculty seed start-up grant of IISc, the Core Research Grant CRG/2018/002200 from the Science and Engineering Research Board, Department of Science and Technology, Government of India and the Infosys Foundation is greatly acknowledged.

References

- [1] **LIGO Scientific, Virgo** Collaboration, B. P. Abbott et al., *Observation of Gravitational Waves from a Binary Black Hole Merger*, *Phys. Rev. Lett.* **116** (2016), no. 6 061102, [[arXiv:1602.03837](#)].
- [2] **LIGO Scientific, Virgo** Collaboration, B. Abbott et al., *GW150914: First results from the search for binary black hole coalescence with Advanced LIGO*, *Phys. Rev. D* **93** (2016), no. 12 122003, [[arXiv:1602.03839](#)].
- [3] **LIGO Scientific, Virgo** Collaboration, B. Abbott et al., *Properties of the Binary Black Hole Merger GW150914*, *Phys. Rev. Lett.* **116** (2016), no. 24 241102, [[arXiv:1602.03840](#)].
- [4] **LIGO Scientific, Virgo** Collaboration, B. P. Abbott et al., *GW151226: Observation of Gravitational Waves from a 22-Solar-Mass Binary Black Hole Coalescence*, *Phys. Rev. Lett.* **116** (2016), no. 24 241103, [[arXiv:1606.04855](#)].
- [5] **LIGO Scientific, Virgo** Collaboration, B. P. Abbott et al., *GW170104: Observation of a 50-Solar-Mass Binary Black Hole Coalescence at Redshift 0.2*, *Phys. Rev. Lett.* **118** (2017), no. 22 221101, [[arXiv:1706.01812](#)]. [Erratum: *Phys. Rev. Lett.* 121, no. 12, 129901 (2018)].
- [6] **LIGO Scientific, Virgo** Collaboration, B. P. Abbott et al., *GW170814: A Three-Detector Observation of Gravitational Waves from a Binary Black Hole Coalescence*, *Phys. Rev. Lett.* **119** (2017), no. 14 141101, [[arXiv:1709.09660](#)].
- [7] **LIGO Scientific, Virgo** Collaboration, B. P. Abbott et al., *Astrophysical Implications of the Binary Black-Hole Merger GW150914*, *Astrophys. J.* **818** (2016), no. 2 L22, [[arXiv:1602.03846](#)].

- [8] K. Belczynski, D. E. Holz, T. Bulik, and R. O’Shaughnessy, *The first gravitational-wave source from the isolated evolution of two 40-100 Msun stars*, *Nature* **534** (2016) 512, [[arXiv:1602.04531](#)].
- [9] N. Duechting, *Supermassive black holes from primordial black hole seeds*, *Phys. Rev.* **D70** (2004) 064015, [[astro-ph/0406260](#)].
- [10] R. Bean and J. Magueijo, *Could supermassive black holes be quintessential primordial black holes?*, *Phys. Rev.* **D66** (2002) 063505, [[astro-ph/0204486](#)].
- [11] S. Hawking, *Gravitationally collapsed objects of very low mass*, *Mon. Not. Roy. Astron. Soc.* **152** (1971) 75.
- [12] B. J. Carr and S. W. Hawking, *Black holes in the early Universe*, *Mon. Not. Roy. Astron. Soc.* **168** (1974) 399–415.
- [13] M. Khlopov, B. A. Malomed, and I. B. Zeldovich, *Gravitational instability of scalar fields and formation of primordial black holes*, *Mon. Not. Roy. Astron. Soc.* **215** (1985) 575–589.
- [14] P. Ivanov, P. Naselsky, and I. Novikov, *Inflation and primordial black holes as dark matter*, *Phys. Rev.* **D50** (1994) 7173–7178.
- [15] J. Garcia-Bellido, A. D. Linde, and D. Wands, *Density perturbations and black hole formation in hybrid inflation*, *Phys. Rev.* **D54** (1996) 6040–6058, [[astro-ph/9605094](#)].
- [16] T. Kawaguchi, M. Kawasaki, T. Takayama, M. Yamaguchi, and J. Yokoyama, *Formation of intermediate-mass black holes as primordial black holes in the inflationary cosmology with running spectral index*, *Mon. Not. Roy. Astron. Soc.* **388** (2008) 1426–1432, [[arXiv:0711.3886](#)].
- [17] K. Kohri, D. H. Lyth, and A. Melchiorri, *Black hole formation and slow-roll inflation*, *JCAP* **0804** (2008) 038, [[arXiv:0711.5006](#)].
- [18] M. Drees and E. Erfani, *Running Spectral Index and Formation of Primordial Black Hole in Single Field Inflation Models*, *JCAP* **1201** (2012) 035, [[arXiv:1110.6052](#)].
- [19] E. Bugaev and P. Klimai, *Formation of primordial black holes from non-Gaussian perturbations produced in a waterfall transition*, *Phys. Rev.* **D85** (2012) 103504, [[arXiv:1112.5601](#)].
- [20] E. Erfani, *Modulated Inflation Models and Primordial Black Holes*, *Phys. Rev.* **D89** (2014), no. 8 083511, [[arXiv:1311.3090](#)].
- [21] S. Clesse and J. Garcia-Bellido, *Massive Primordial Black Holes from Hybrid Inflation as Dark Matter and the seeds of Galaxies*, *Phys. Rev.* **D92** (2015), no. 2 023524, [[arXiv:1501.07565](#)].
- [22] E. Erfani, *Primordial Black Holes Formation from Particle Production during Inflation*, *JCAP* **1604** (2016), no. 04 020, [[arXiv:1511.08470](#)].
- [23] J. Garcia-Bellido and E. Ruiz Morales, *Primordial black holes from single field models of inflation*, *Phys. Dark Univ.* **18** (2017) 47–54, [[arXiv:1702.03901](#)].
- [24] J. M. Ezquiaga, J. Garcia-Bellido, and E. Ruiz Morales, *Primordial Black Hole production in Critical Higgs Inflation*, *Phys. Lett.* **B776** (2018) 345–349, [[arXiv:1705.04861](#)].
- [25] K. Kannike, L. Marzola, M. Raidal, and H. Veermae, *Single Field Double Inflation and Primordial Black Holes*, *JCAP* **1709** (2017), no. 09 020, [[arXiv:1705.06225](#)].
- [26] G. Ballesteros and M. Taoso, *Primordial black hole dark matter from single field inflation*, *Phys. Rev.* **D97** (2018), no. 2 023501, [[arXiv:1709.05565](#)].
- [27] M. P. Hertzberg and M. Yamada, *Primordial Black Holes from Polynomial Potentials in Single Field Inflation*, *Phys. Rev.* **D97** (2018), no. 8 083509, [[arXiv:1712.09750](#)].
- [28] S. Pi, Y.-l. Zhang, Q.-G. Huang, and M. Sasaki, *Scalaron from R^2 -gravity as a heavy field*,

- JCAP* **1805** (2018), no. 05 042, [[arXiv:1712.09896](#)].
- [29] M. Cicoli, V. A. Diaz, and F. G. Pedro, *Primordial Black Holes from String Inflation*, *JCAP* **1806** (2018), no. 06 034, [[arXiv:1803.02837](#)].
- [30] A. Y. Kamenshchik, A. Tronconi, T. Vardanyan, and G. Venturi, *Non-Canonical Inflation and Primordial Black Holes Production*, *Phys. Lett.* **B791** (2019) 201–205, [[arXiv:1812.02547](#)].
- [31] K. Dimopoulos, T. Markkanen, A. Racioppi, and V. Vaskonen, *Primordial Black Holes from Thermal Inflation*, *JCAP* **1907** (2019) 046, [[arXiv:1903.09598](#)].
- [32] N. Bhaumik and R. K. Jain, *Primordial black holes dark matter from inflection point models of inflation and the effects of reheating*, *JCAP* **01** (2020) 037, [[arXiv:1907.04125](#)].
- [33] V. Atal, J. Cid, A. Escriv, and J. Garriga, *PBH in single field inflation: the effect of shape dispersion and non-Gaussianities*, *JCAP* **05** (2020) 022, [[arXiv:1908.11357](#)].
- [34] S. S. Mishra and V. Sahni, *Primordial Black Holes from a tiny bump/dip in the Inflaton potential*, *JCAP* **04** (2020) 007, [[arXiv:1911.00057](#)].
- [35] G. Ballesteros, J. Rey, M. Taoso, and A. Urbano, *Primordial black holes as dark matter and gravitational waves from single-field polynomial inflation*, *JCAP* **07** (2020) 025, [[arXiv:2001.08220](#)].
- [36] P. ConzINU, M. Gasperini, and G. Marozzi, *Primordial Black Holes from Pre-Big Bang inflation*, *JCAP* **08** (2020) 031, [[arXiv:2004.08111](#)].
- [37] M. Braglia, D. K. Hazra, F. Finelli, G. F. Smoot, L. Sriramkumar, and A. A. Starobinsky, *Generating PBHs and small-scale GWs in two-field models of inflation*, *JCAP* **08** (2020) 001, [[arXiv:2005.02895](#)].
- [38] A. A. Starobinsky, *Spectrum of relict gravitational radiation and the early state of the universe*, *JETP Lett.* **30** (1979) 682–685.
- [39] L. A. Boyle and P. J. Steinhardt, *Probing the early universe with inflationary gravitational waves*, *Phys. Rev. D* **77** (2008) 063504, [[astro-ph/0512014](#)].
- [40] R. Durrer and J. Hasenkamp, *Testing Superstring Theories with Gravitational Waves*, *Phys. Rev. D* **84** (2011) 064027, [[arXiv:1105.5283](#)].
- [41] S. Kuroyanagi, T. Chiba, and N. Sugiyama, *Prospects for Direct Detection of Inflationary Gravitational Waves by Next Generation Interferometric Detectors*, *Phys. Rev. D* **83** (2011) 043514, [[arXiv:1010.5246](#)].
- [42] K. D. Lozanov and M. A. Amin, *Equation of State and Duration to Radiation Domination after Inflation*, *Phys. Rev. Lett.* **119** (2017), no. 6 061301, [[arXiv:1608.01213](#)].
- [43] D. G. Figueroa and E. H. Tanin, *Ability of LIGO and LISA to probe the equation of state of the early Universe*, *JCAP* **08** (2019) 011, [[arXiv:1905.11960](#)].
- [44] M. Guzzetti, N. Bartolo, M. Liguori, and S. Matarrese, *Gravitational waves from inflation*, *Riv. Nuovo Cim.* **39** (2016), no. 9 399–495, [[arXiv:1605.01615](#)].
- [45] C. Caprini and D. G. Figueroa, *Cosmological Backgrounds of Gravitational Waves*, *Class. Quant. Grav.* **35** (2018), no. 16 163001, [[arXiv:1801.04268](#)].
- [46] K. N. Ananda, C. Clarkson, and D. Wands, *The Cosmological gravitational wave background from primordial density perturbations*, *Phys. Rev. D* **75** (2007) 123518, [[gr-qc/0612013](#)].
- [47] D. Baumann, P. J. Steinhardt, K. Takahashi, and K. Ichiki, *Gravitational Wave Spectrum Induced by Primordial Scalar Perturbations*, *Phys. Rev. D* **76** (2007) 084019, [[hep-th/0703290](#)].
- [48] R. Saito and J. Yokoyama, *Gravitational wave background as a probe of the primordial black hole abundance*, *Phys. Rev. Lett.* **102** (2009) 161101, [[arXiv:0812.4339](#)]. [Erratum:

Phys.Rev.Lett. 107, 069901 (2011)].

- [49] L. Alabidi, K. Kohri, M. Sasaki, and Y. Sendouda, *Observable Spectra of Induced Gravitational Waves from Inflation*, *JCAP* **09** (2012) 017, [[arXiv:1203.4663](#)].
- [50] L. Alabidi, K. Kohri, M. Sasaki, and Y. Sendouda, *Observable induced gravitational waves from an early matter phase*, *JCAP* **05** (2013) 033, [[arXiv:1303.4519](#)].
- [51] T. Nakama, J. Silk, and M. Kamionkowski, *Stochastic gravitational waves associated with the formation of primordial black holes*, *Phys. Rev. D* **95** (2017), no. 4 043511, [[arXiv:1612.06264](#)].
- [52] K. Kohri and T. Terada, *Semianalytic calculation of gravitational wave spectrum nonlinearly induced from primordial curvature perturbations*, *Phys. Rev. D* **97** (2018), no. 12 123532, [[arXiv:1804.08577](#)].
- [53] N. Bartolo, V. De Luca, G. Franciolini, A. Lewis, M. Peloso, and A. Riotto, *Primordial Black Hole Dark Matter: LISA Serendipity*, *Phys. Rev. Lett.* **122** (2019), no. 21 211301, [[arXiv:1810.12218](#)].
- [54] N. Bartolo, V. De Luca, G. Franciolini, M. Peloso, D. Racco, and A. Riotto, *Testing primordial black holes as dark matter with LISA*, *Phys. Rev. D* **99** (2019), no. 10 103521, [[arXiv:1810.12224](#)].
- [55] K. Inomata and T. Nakama, *Gravitational waves induced by scalar perturbations as probes of the small-scale primordial spectrum*, *Phys. Rev. D* **99** (2019), no. 4 043511, [[arXiv:1812.00674](#)].
- [56] S. Clesse, J. Garcia-Bellido, and S. Orani, *Detecting the Stochastic Gravitational Wave Background from Primordial Black Hole Formation*, [arXiv:1812.11011](#).
- [57] F. Hajkarim and J. Schaffner-Bielich, *Thermal History of the Early Universe and Primordial Gravitational Waves from Induced Scalar Perturbations*, *Phys. Rev. D* **101** (2020), no. 4 043522, [[arXiv:1910.12357](#)].
- [58] C. Fu, P. Wu, and H. Yu, *Scalar induced gravitational waves in inflation with gravitationally enhanced friction*, *Phys. Rev. D* **101** (2020), no. 2 023529, [[arXiv:1912.05927](#)].
- [59] J. Lin, Q. Gao, Y. Gong, Y. Lu, C. Zhang, and F. Zhang, *Primordial black holes and secondary gravitational waves from k and G inflation*, *Phys. Rev. D* **101** (2020), no. 10 103515, [[arXiv:2001.05909](#)].
- [60] G. Domenech, S. Pi, and M. Sasaki, *Induced gravitational waves as a probe of thermal history of the universe*, *JCAP* **08** (2020) 017, [[arXiv:2005.12314](#)].
- [61] I. Dalianis and K. Kritos, *Exploring the Spectral Shape of Gravitational Waves Induced by Primordial Scalar Perturbations and Connection with the Primordial Black Hole Scenarios*, [arXiv:2007.07915](#).
- [62] H. Ragavendra, P. Saha, L. Sriramkumar, and J. Silk, *PBHs and secondary GWs from ultra slow roll and punctuated inflation*, [arXiv:2008.12202](#).
- [63] K. Danzmann, *LISA: An ESA cornerstone mission for a gravitational wave observatory*, *Class. Quant. Grav.* **14** (1997) 1399–1404.
- [64] B. Sathyaprakash and B. Schutz, *Physics, Astrophysics and Cosmology with Gravitational Waves*, *Living Rev. Rel.* **12** (2009) 2, [[arXiv:0903.0338](#)].
- [65] N. Bartolo et al., *Science with the space-based interferometer LISA. IV: Probing inflation with gravitational waves*, *JCAP* **12** (2016) 026, [[arXiv:1610.06481](#)].
- [66] **LISA** Collaboration, P. Amaro-Seoane et al., *Laser Interferometer Space Antenna*, [arXiv:1702.00786](#).

- [67] W.-H. Ruan, Z.-K. Guo, R.-G. Cai, and Y.-Z. Zhang, *Taiji Program: Gravitational-Wave Sources*, *Int. J. Mod. Phys. A* **35** (2020), no. 17 2050075, [[arXiv:1807.09495](#)].
- [68] N. Seto, S. Kawamura, and T. Nakamura, *Possibility of direct measurement of the acceleration of the universe using 0.1-Hz band laser interferometer gravitational wave antenna in space*, *Phys. Rev. Lett.* **87** (2001) 221103, [[astro-ph/0108011](#)].
- [69] K. Yagi and N. Seto, *Detector configuration of DECIGO/BBO and identification of cosmological neutron-star binaries*, *Phys. Rev. D* **83** (2011) 044011, [[arXiv:1101.3940](#)]. [Erratum: *Phys.Rev.D* 95, 109901 (2017)].
- [70] V. Corbin and N. J. Cornish, *Detecting the cosmic gravitational wave background with the big bang observer*, *Class. Quant. Grav.* **23** (2006) 2435–2446, [[gr-qc/0512039](#)].
- [71] **LIGO Scientific** Collaboration, J. Aasi et al., *Advanced LIGO*, *Class. Quant. Grav.* **32** (2015) 074001, [[arXiv:1411.4547](#)].
- [72] J. R. Espinosa, D. Racco, and A. Riotto, *A Cosmological Signature of the SM Higgs Instability: Gravitational Waves*, *JCAP* **09** (2018) 012, [[arXiv:1804.07732](#)].
- [73] C. T. Byrnes, P. S. Cole, and S. P. Patil, *Steepest growth of the power spectrum and primordial black holes*, *JCAP* **1906** (2019), no. 06 028, [[arXiv:1811.11158](#)].
- [74] P. Carrilho, K. A. Malik, and D. J. Mulryne, *Dissecting the growth of the power spectrum for primordial black holes*, *Phys. Rev. D* **100** (2019), no. 10 103529, [[arXiv:1907.05237](#)].
- [75] L. Lentati et al., *European Pulsar Timing Array Limits On An Isotropic Stochastic Gravitational-Wave Background*, *Mon. Not. Roy. Astron. Soc.* **453** (2015), no. 3 2576–2598, [[arXiv:1504.03692](#)].
- [76] R. Shannon et al., *Gravitational waves from binary supermassive black holes missing in pulsar observations*, *Science* **349** (2015), no. 6255 1522–1525, [[arXiv:1509.07320](#)].
- [77] C. Yuan, Z.-C. Chen, and Q.-G. Huang, *Log-dependent slope of scalar induced gravitational waves in the infrared regions*, *Phys. Rev. D* **101** (2020), no. 4 043019, [[arXiv:1910.09099](#)].
- [78] R.-G. Cai, S. Pi, and M. Sasaki, *Universal infrared scaling of gravitational wave background spectra*, [arXiv:1909.13728](#).
- [79] W.-T. Xu, J. Liu, T.-J. Gao, and Z.-K. Guo, *Gravitational waves from double-inflection-point inflation*, *Phys. Rev. D* **101** (2020), no. 2 023505, [[arXiv:1907.05213](#)].
- [80] J. Liu, Z.-K. Guo, and R.-G. Cai, *Analytical approximation of the scalar spectrum in the ultraslow-roll inflationary models*, *Phys. Rev. D* **101** (2020), no. 8 083535, [[arXiv:2003.02075](#)].
- [81] B. J. Carr, K. Kohri, Y. Sendouda, and J. Yokoyama, *New cosmological constraints on primordial black holes*, *Phys. Rev.* **D81** (2010) 104019, [[arXiv:0912.5297](#)].
- [82] B. Carr and F. Kuhnel, *Primordial Black Holes as Dark Matter: Recent Developments*, [arXiv:2006.02838](#).
- [83] R. Laha, *Primordial Black Holes as a Dark Matter Candidate Are Severely Constrained by the Galactic Center 511 keV γ -Ray Line*, *Phys. Rev. Lett.* **123** (2019), no. 25 251101, [[arXiv:1906.09994](#)].
- [84] J. Garcia-Bellido, M. Peloso, and C. Unal, *Gravitational Wave signatures of inflationary models from Primordial Black Hole Dark Matter*, *JCAP* **1709** (2017), no. 09 013, [[arXiv:1707.02441](#)].
- [85] B. J. Carr, *The Primordial black hole mass spectrum*, *Astrophys. J.* **201** (1975) 1–19.
- [86] S. J. Kapadia, K. L. Pandey, T. Suyama, and P. Ajith, *Prospects for probing ultralight primordial black holes using the stochastic gravitational-wave background induced by primordial*

- curvature perturbations, *Phys. Rev. D* **101** (2020), no. 12 123535, [[arXiv:2005.05693](#)].
- [87] A. R. Liddle and S. M. Leach, *How long before the end of inflation were observable perturbations produced?*, *Phys. Rev. D* **68** (2003) 103503, [[astro-ph/0305263](#)].
- [88] K. Inomata, M. Kawasaki, K. Mukaida, T. Terada, and T. T. Yanagida, *Gravitational Wave Production right after a Primordial Black Hole Evaporation*, *Phys. Rev. D* **101** (2020), no. 12 123533, [[arXiv:2003.10455](#)].
- [89] J. F. Dufaux, A. Bergman, G. N. Felder, L. Kofman, and J.-P. Uzan, *Theory and Numerics of Gravitational Waves from Preheating after Inflation*, *Phys. Rev. D* **76** (2007) 123517, [[arXiv:0707.0875](#)].
- [90] R. K. Jain, P. Chingangbam, and L. Sriramkumar, *On the evolution of tachyonic perturbations at super-Hubble scales*, *JCAP* **0710** (2007) 003, [[astro-ph/0703762](#)].
- [91] R. K. Jain, P. Chingangbam, J.-O. Gong, L. Sriramkumar, and T. Souradeep, *Punctuated inflation and the low CMB multipoles*, *JCAP* **0901** (2009) 009, [[arXiv:0809.3915](#)].
- [92] R. K. Jain, P. Chingangbam, L. Sriramkumar, and T. Souradeep, *The tensor-to-scalar ratio in punctuated inflation*, *Phys. Rev.* **D82** (2010) 023509, [[arXiv:0904.2518](#)].
- [93] R. Durrer, L. Hollenstein, and R. K. Jain, *Can slow roll inflation induce relevant helical magnetic fields?*, *JCAP* **03** (2011) 037, [[arXiv:1005.5322](#)].
- [94] C. T. Byrnes, L. Hollenstein, R. K. Jain, and F. R. Urban, *Resonant magnetic fields from inflation*, *JCAP* **03** (2012) 009, [[arXiv:1111.2030](#)].
- [95] R. K. Jain and M. S. Sloth, *Consistency relation for cosmic magnetic fields*, *Phys. Rev. D* **86** (2012) 123528, [[arXiv:1207.4187](#)].
- [96] R. K. Jain and M. S. Sloth, *On the non-Gaussian correlation of the primordial curvature perturbation with vector fields*, *JCAP* **02** (2013) 003, [[arXiv:1210.3461](#)].
- [97] A. Maleknejad, M. Sheikh-Jabbari, and J. Soda, *Gauge Fields and Inflation*, *Phys. Rept.* **528** (2013) 161–261, [[arXiv:1212.2921](#)].
- [98] R. J. Z. Ferreira, R. K. Jain, and M. S. Sloth, *Inflationary magnetogenesis without the strong coupling problem*, *JCAP* **1310** (2013) 004, [[arXiv:1305.7151](#)].
- [99] R. J. Ferreira, R. K. Jain, and M. S. Sloth, *Inflationary Magnetogenesis without the Strong Coupling Problem II: Constraints from CMB anisotropies and B-modes*, *JCAP* **06** (2014) 053, [[arXiv:1403.5516](#)].
- [100] O. Özsoy, *Gravitational Waves from a Rolling Axion Monodromy*, [arXiv:2005.10280](#).
- [101] O. Özsoy and Z. Lalak, *Primordial black holes as dark matter and gravitational waves from axion inflation*, [arXiv:2008.07549](#).
- [102] S. Clesse and J. Garca-Bellido, *Detecting the gravitational wave background from primordial black hole dark matter*, *Phys. Dark Univ.* **18** (2017) 105–114, [[arXiv:1610.08479](#)].
- [103] V. Mandic, S. Bird, and I. Cholis, *Stochastic Gravitational-Wave Background due to Primordial Binary Black Hole Mergers*, *Phys. Rev. Lett.* **117** (2016), no. 20 201102, [[arXiv:1608.06699](#)].
- [104] **LIGO Scientific, Virgo** Collaboration, R. Abbott et al., *GW190521: A Binary Black Hole Merger with a Total Mass of $150 M_{\odot}$* , *Phys. Rev. Lett.* **125** (2020), no. 10 101102, [[arXiv:2009.01075](#)].
- [105] **LIGO Scientific, Virgo** Collaboration, R. Abbott et al., *Properties and astrophysical implications of the $150 M_{\text{sun}}$ binary black hole merger GW190521*, *Astrophys. J. Lett.* **900** (2020) L13, [[arXiv:2009.01190](#)].
- [106] K. Tomikawa and T. Kobayashi, *Gauge dependence of gravitational waves generated at second*

- order from scalar perturbations, *Phys. Rev. D* **101** (2020), no. 8 083529, [[arXiv:1910.01880](#)].
- [107] V. De Luca, G. Franciolini, A. Kehagias, and A. Riotto, *On the Gauge Invariance of Cosmological Gravitational Waves*, *JCAP* **03** (2020) 014, [[arXiv:1911.09689](#)].
- [108] K. Inomata and T. Terada, *Gauge Independence of Induced Gravitational Waves*, *Phys. Rev. D* **101** (2020), no. 2 023523, [[arXiv:1912.00785](#)].
- [109] C. Yuan, Z.-C. Chen, and Q.-G. Huang, *Scalar induced gravitational waves in different gauges*, *Phys. Rev. D* **101** (2020), no. 6 063018, [[arXiv:1912.00885](#)].
- [110] Y. Lu, A. Ali, Y. Gong, J. Lin, and F. Zhang, *On the gauge transformation of scalar induced gravitational waves*, [[arXiv:2006.03450](#)].
- [111] L. Bethke, D. G. Figueroa, and A. Rajantie, *Anisotropies in the Gravitational Wave Background from Preheating*, *Phys. Rev. Lett.* **111** (2013), no. 1 011301, [[arXiv:1304.2657](#)].
- [112] M. Geller, A. Hook, R. Sundrum, and Y. Tsai, *Primordial Anisotropies in the Gravitational Wave Background from Cosmological Phase Transitions*, *Phys. Rev. Lett.* **121** (2018), no. 20 201303, [[arXiv:1803.10780](#)].
- [113] C. R. Contaldi, *Anisotropies of Gravitational Wave Backgrounds: A Line Of Sight Approach*, *Phys. Lett. B* **771** (2017) 9–12, [[arXiv:1609.08168](#)].
- [114] N. Bartolo, D. Bertacca, S. Matarrese, M. Peloso, A. Ricciardone, A. Riotto, and G. Tasinato, *Anisotropies and non-Gaussianity of the Cosmological Gravitational Wave Background*, *Phys. Rev. D* **100** (2019), no. 12 121501, [[arXiv:1908.00527](#)].
- [115] N. Bartolo, D. Bertacca, S. Matarrese, M. Peloso, A. Ricciardone, A. Riotto, and G. Tasinato, *Characterizing the cosmological gravitational wave background: Anisotropies and non-Gaussianity*, *Phys. Rev. D* **102** (2020), no. 2 023527, [[arXiv:1912.09433](#)].
- [116] V. Domcke, R. Jinno, and H. Rubira, *Deformation of the gravitational wave spectrum by density perturbations*, *JCAP* **06** (2020) 046, [[arXiv:2002.11083](#)].
- [117] N. Bartolo, D. Bertacca, V. De Luca, G. Franciolini, S. Matarrese, M. Peloso, A. Ricciardone, A. Riotto, and G. Tasinato, *Gravitational wave anisotropies from primordial black holes*, *JCAP* **02** (2020) 028, [[arXiv:1909.12619](#)].
- [118] M. Gertsenshtein, *Wave Resonance of Light and Gravitational Waves*, *Sov. Phys. JETP* **14** (1962) 84.
- [119] Y. B. Zel'dovich, *Electromagnetic and gravitational waves in a stationary magnetic field*, *Sov. Phys. JETP* **38** (1974) 652.
- [120] A. D. Dolgov and D. Ejlli, *Relic gravitational waves from light primordial black holes*, *Phys. Rev. D* **84** (2011) 024028, [[arXiv:1105.2303](#)].
- [121] A. Ejlli, D. Ejlli, A. M. Cruise, G. Pisano, and H. Grote, *Upper limits on the amplitude of ultra-high-frequency gravitational waves from graviton to photon conversion*, *Eur. Phys. J. C* **79** (2019), no. 12 1032, [[arXiv:1908.00232](#)].
- [122] V. Domcke and C. Garcia-Cely, *The CMB Rayleigh-Jeans tail as a detector of high-frequency gravitational waves*, [[arXiv:2006.01161](#)].
- [123] **NANOGrav** Collaboration, Z. Arzoumanian et al., *The NANOGrav 12.5-year Data Set: Search For An Isotropic Stochastic Gravitational-Wave Background*, [[arXiv:2009.04496](#)].
- [124] V. Vaskonen and H. Veermäe, *Did NANOGrav see a signal from primordial black hole formation?*, [[arXiv:2009.07832](#)].
- [125] V. De Luca, G. Franciolini, and A. Riotto, *NANOGrav Hints to Primordial Black Holes as Dark Matter*, [[arXiv:2009.08268](#)].